Investigation of Molecular Mechanism of Transthyretin Oligomerization Associated with ATTR Amyloidosis

by

Matthew Fontaine Coats

May, 2022

Director of Thesis: Dr. Kwang Hun Lim

Major Department: Chemistry

Transthyretin amyloidosis (ATTR) has classically been diagnosed predominantly post-observation of amyloid fibril deposition on soft tissues within the body, however, recent studies have shown that oligomers which arise during the aggregation process are much more cytotoxic than their amyloid fibril counterparts.[2,6,7] Additionally, it has also been found that cleaved C-terminal fragments, within the peptide range of T49-E127, circulate in-vivo with these oligomers and amyloids, providing further insight into the vast complexity of amyloidogenic species circulating within patients.[5,11] Previous mechanistic studies of transthyretin misfolding and aggregation have shed light on the capability of the native protein to first dissociate into its constituent monomers, which are then capable of self-associating into dimeric species that subsequently form hexamers and eventually large cytotoxic oligomers.[2,6,9] Whilst searching for the specific amino acid sequences involved in amyloidosis within ATTR, it was found that mutations E92P, in the A91-T96 peptide chain, or T119W, in the T119-N124 peptide chain, were both able to completely inhibit aggregation.[23] This study seeks to examine the specific molecular mechanism behind transthyretin dimerization in misfolding pathways by introducing the E92P and T119W mutations directly into the H-H’ and F-F’ β-strand of the native dimeric interface of TTR.

Structural characterization profiles of non-native TTR species which arise during the

aggregation process of wild-type TTR (WT-TTR), as well as those of the highly amyloidogenic mutations V30M and L55P were propagated under acidic and kinetically favorable conditions to induce aggregation while maintaining an observable timeline. The WT and mutant forms of TTR underwent similar aggregation processes, involving large concentrations of tetramers first dissociating into monomers, these misfolded monomers then form misfolded dimers, and at the peak of dimer formation high molecular weight oligomers begin to form. These observations indicate the importance of the misfolded monomer's ability to form into misfolded dimers with regards to the eventual formation of oligomeric species. In order to examine if the native dimeric interface sites, along the H-H' and F-F' β-strand bonds, are integral parts of WT-TTR and L55P-TTR's ability to aggregate into misfolded dimeric species, proline substitutions were introduced into the E92 peptide within their F-strands as well as tryptophan substitutions into the T119 peptide within their H-strands. These two bulky peptide substitutions showed clear inhibition of non-native oligomeric species under acidic conditions as well as in samples which had been proteolytically cleaved at the L48-T49 peptide bond using trypsin digestion. As these mutations may be having a stabilizing effect on the native tetramer during the dissociation phase, rather than the intended inhibitory effect during the aggregation phase, leading to the observed decrease in oligomerization, a monomeric variant of TTR (m-TTR) was also studied in similar fashion to the WT-TTR and L55P-TTR trials. Similar to the previous wild-type and L55P studies, the inhibited m-TTR samples proved successful in eliminating dimerization. These results indicate that oligomerization of TTR is dependent upon the ability of its dissociated misfolded monomers to form into misfolded dimers, and by introducing large sidechains into locations within the dimeric interface, it is possible to eliminate the ability of these misfolded monomers to aggregate into larger amyloidogenic species.

Investigation of Molecular Mechanism of Transthyretin Oligomerization Associated with ATTR Amyloidosis

A Thesis

Presented to the Faculty of the Department of Chemistry

East Carolina University

In Partial Fulfillment of the Requirements for the Degree

Master's of Science in Chemistry

by

Matthew Fontaine Coats

May, 2022

Investigation of Molecular Mechanism of Transthyretin Oligomerization Associated with ATTR Amyloidosis

By: Matthew Fontaine Coats

APPROVED BY:

DIRECTOR OF THESIS	Kwang Hun Lim, Ph.D.
COMMITTEE MEMBER	Colin Burns, Ph. D.
COMMITTEE MEMBER	Robert M. Hughes, Ph. D.
CHAIR OF THE DEPARTMENT OF CHEMISTRY	Andrew T. Morehead, Jr., Ph. D.
DEAN OF THE GRADUATE SCHOOL	Paul Gemperline, Ph. D.

TABLE OF CONTENTS

LIST OF FIGURES

LIST OF ABBREVIATIONS

ANION EXCHANGE CHROMATOGRAPHY	AEC
FAMILIAL AMYLOIDOTIC CARDIOMYOPATHY	FAC
FAMILIAL AMYLOIDOTIC POLYNEUROPATHY	FAP
FAST PASS LIQUID CHROMATOGRAPHY	FPLC
HEREDITARY TRANSTHYRETIN AMYLOIDOSIS	hATTR
HOLO-RETINOL BINDING PROTEIN	RBP
MONOMERIC TRANSTHYRETIN	m-TTR
OPTICAL DENSITY AT 400nm	OD_{400}
PHOSPHATE-BUFFERED SALINE	PBS
ROTATIONS PER MINUTE	RPM
SENILE SYSTEMIC AMYLOIDOSIS	SSA
SIZE EXCLUSION CHROMATOGRAPHY	SEC
THIOFLAVIN T	ThT
THYROXINE	T4
TRANSTHYRETIN	TTR
TRANSTHYRETIN AMYLOIDOSIS	ATTR
WILD-TYPE TRANSTHYRETIN	WT-TTR

Chapter 1: Introduction

1.1 Protein Folding and Misfolding

Proteins are one of the most diverse complex biological molecules found in virtually every form of life on earth. They are essential in key physiological processes ranging from the transportation of smaller molecules and atoms, transmission of biological signals, building cellular structures, carrying out necessary biochemical reactions and providing defense against pathogens. Occasionally, errors occur in the protein folding process, resulting in misfolded proteins which are recognized by the cells quality control systems and discarded of. These discarded misfolded proteins are mostly broken back down and recycled, however, some are not recaptured and accumulate within the cell, where they are able to aggregate with other similarly misfolded proteins. During the aggregation process, the misfolded proteins are able to form into amorphous aggregates, oligomers, and amyloid fibrils (Figure 1.1).[2,9] These non-native species are then deposited onto various soft tissues and organs, causing detrimental effects to the affected areas.[2]

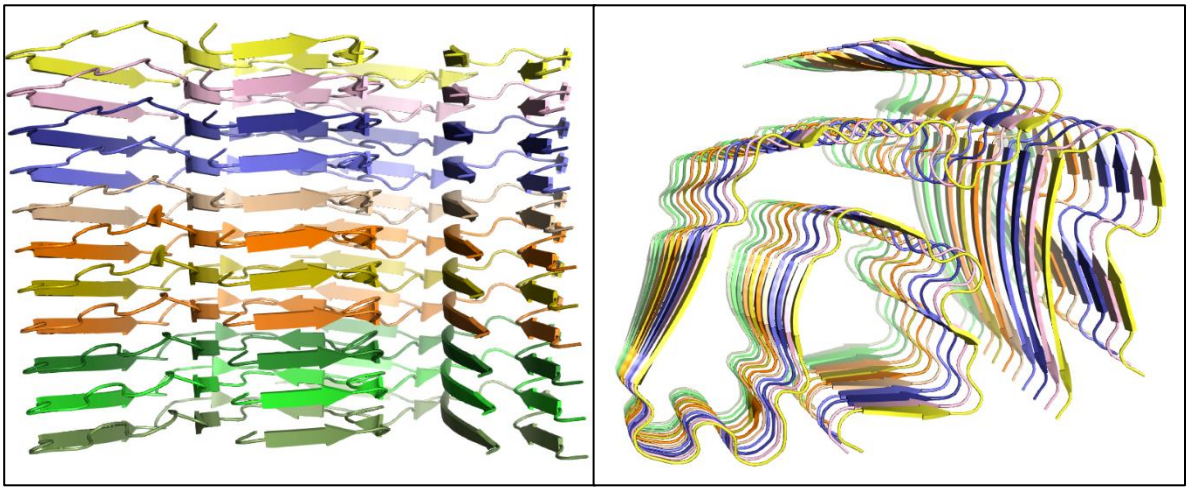

Figure 1.1 Example of amyloid spine consisting of stacked β-strands from a patient suffering from ATTR stemming from the V30M mutation.

1.2 Amyloids and Amyloidosis

Amyloid fibrils have a unique morphology that has been examined under X-ray diffraction showing patterns of a cross-β spine composed of beta pleated sheets with the β-sheets having their extended protein strand perpendicular to the axis and β-sheets parallel to the axis (Figure 1.1).[24] The amyloid state of a protein has been shown to be the universal free-energy ground state, making it theoretically accessible for all proteins and is characterized by the steric zippers of the cross-β spine (Figure 1.2).[13,24] While undergoing normal physiological aggregation, misfolded proteins are susceptible to primary and secondary nucleation aggregation kinetics which leads to the formation of cytotoxic oligomers, protofibrils, and eventually fully developed amyloid fibrils.[2,6,24]

Amyloidosis is a disease characterized as having developed from the deposition of elongated, unbranched protein fibrils on soft tissues or organs within the body.[7] In order for a disease to be classified as a form of amyloidosis, the fibrils must be given an “apple-green” birefringence when binding to the dye Congo Red.[7] Amyloid fibrils have also been shown to exhibit enhanced Thioflavin T (ThT) fluorescence upon binding with ThT. [2,7]

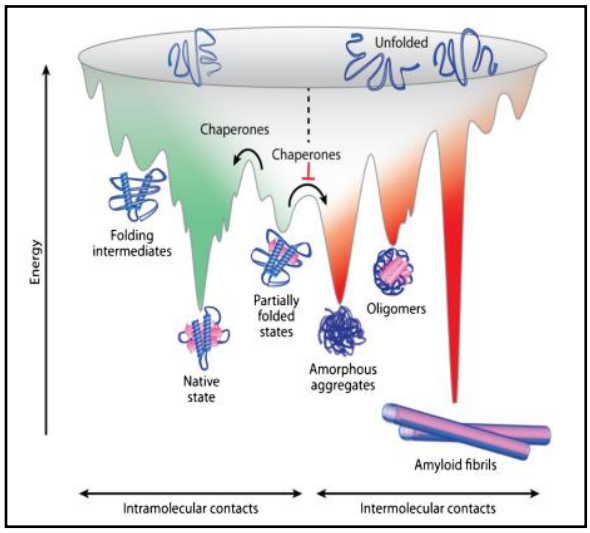

Figure 1.2 Energy landscape of amyloidosis. Adopted from A. C. Muntau “Innovative strategies to treat protein misfolding in inborn errors of metabolism: pharmacological chaperones and proteostasis regulators.”

Currently, there are over 40 recorded precursor proteins confirmed to be in amyloid protein fibrils found in patients affected by amyloidosis.[1] The amyloid fibrils associated with the patient's amyloidosis may be hereditary in nature or acquired naturally and they have been found to be deposited both locally and/or systemically.[1] This broad range of means to acquire amyloidosis coupled with the uniqueness of each patient's diagnosis makes early detection and treatment incredibly arduous. Hereditary ATTR (hATTR) is typically characterized by autosomal-dominant mutations which accelerate the dissociation of the native tetrameric transthyretin and pathological disease progression.[21] ATTR has been linked to three main conditions targeting the peripheral nervous system and heart commonly referred to as senile systemic amyloidosis (SSA), familial amyloidotic cardiomyopathy (FAC), and familial amyloidotic polyneuropathy (FAP).[23] SSA is a late onset disease involving the wild-type (WT) strain of TTR depositing amyloidogenic aggregates on heart tissues and is typically only diagnosed post-mortem on patients 80 years of age or older.[23] FAC and FAP are both hereditary diseases that are characterized by extracellular deposits of TTR variants on the peripheral nerves and heart respectively.[23] FAC is linked to the TTR mutation V122I while FAP has been found to involve several mutations, most commonly at the L55P and V30M positions.[23] Presently, there is no permanent cure for ATTR, however, there are therapeutical treatment methods which involve risky liver transplant surgery or regimented non-steroidal anti-inflammatory medications such as tafamidis or diflunisal, which have both been shown to actively stabilize native TTR tetramers.[2,13,23] Taking into consideration the incredibly vast quantity of people affected by amyloidosis, all of whom are suffering from a wide spectrum of symptoms and being offered a lack of effective treatment, it is easy to see why these diseases, and to a much deeper extent the proteins behind them, need to be investigated further.

1.3 Transthyretin

Originally called prealbumin, due to its closer migration towards the anode in serum protein electrophoresis studies, transthyretin (TTR) is a 55 kDa transport protein which exists natively in a tetrameric state composed of four identical monomers, consisting of 127 amino acids each (Figure 1.3).[2,9] Monomeric TTR consists of eight β-strands split into two β-sheets (DAGH and CBEF) separated by a distance of ≈10 Å (Figure 1.3b).[3] While there is an alpha helix located between Lys76 and Gly83 and several random coils, the overall secondary structure of the TTR monomer is defined as mainly-β with its most predominant topology being that of a β-sandwich.[3,8,23] TTR is introduced naturally into the bloodstream post-synthesis via the liver, with minute amounts having been found secreted into the cerebrospinal fluid through the choroid plexus, and its main physiological purposes are acting as a tertiary carrier of thyroxine (T_4) and holo-retinol binding protein (RBP) (Figure 1.4a & 1.4b).[8,23] While there are two planes of symmetry in which the native TTR tetramer may dissociate into dimers, the most stable form of the TTR dimer has been shown to be formed through symmetrically bound monomers at the H-H' and F-F' binding site, where the prime denotes the opposing monomers β-strand (Figure 1.5).[3,7,23] All of the strands share an anti-parallel symmetry with each other besides strands A and G, giving TTR a uniquely organized characteristic amongst most all-β proteins currently documented.[3]

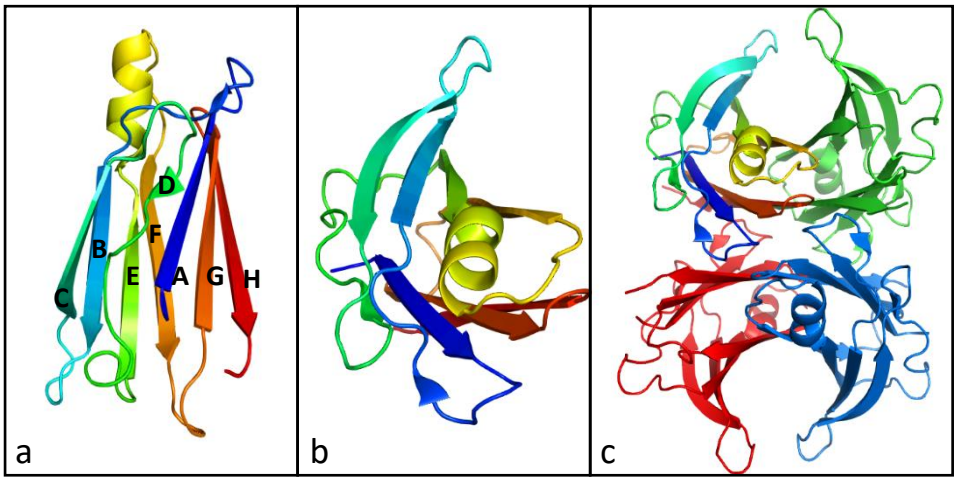

Figure 1.3 (a) X-ray crystal structure of monomeric TTR illustrated as a front facing truncated cylindrical pyramid with individual β-strands A-H independently labeled and colored. (b) Figure 1.3a rotated forward along its x-axis by 90° to demonstrate how the monomer fits into the tetramer. (c) TTR in its native tetrameric state with one of four monomers colored following the scheme from Figures 1.3a and 1.3b.

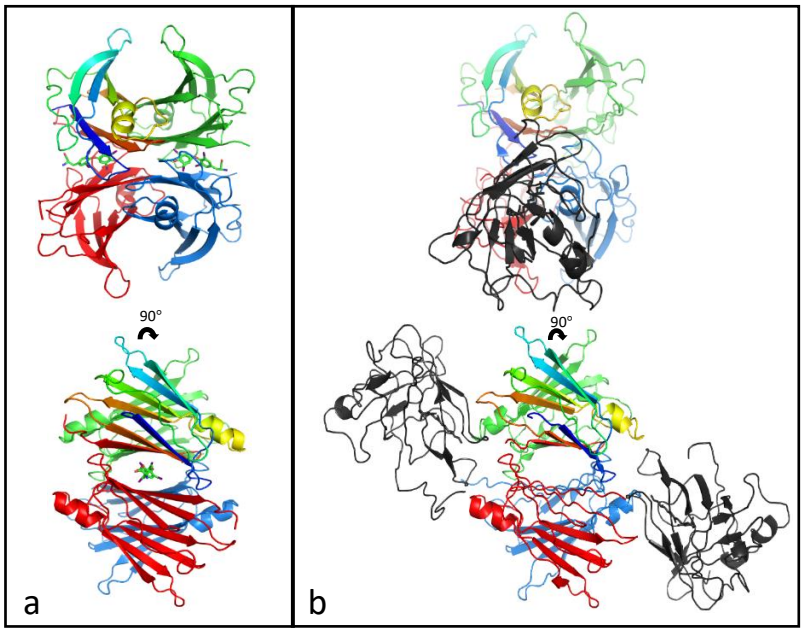

Figure 1.4 (a) Front and side view of thyroxine (T4) binding in the hydrophobic channel of a native TTR tetramer. (b) Front and side view of retinol-binding protein (RBP) binding through AB loop interactions of native TTR tetramer.

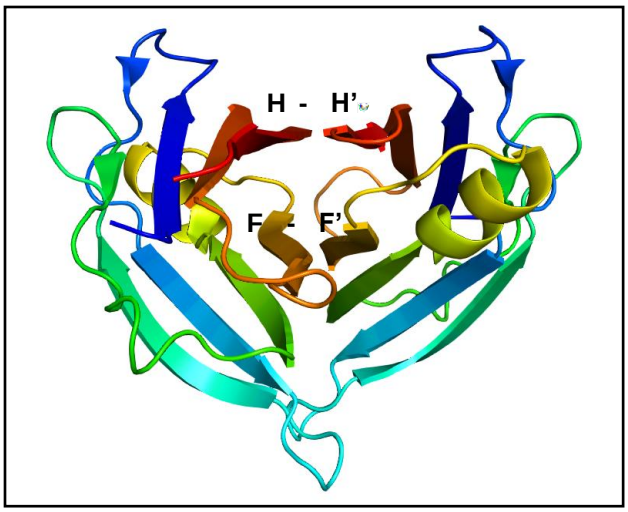

Figure 1.5 3-dimensional crystal structure of two monomeric TTR β–sandwiches bonding through their H and F strands to form a symmetrical dimer.

Dimeric TTR is formed through two monomers bonding their H to H' and F to F' strands in monomers DAGH-CBEF and D'A'G'H'-C'B'E'F' respectively.[3] Each monomer interface, H to H' and F to F', share a total of six hydrogen bonds.[3] Despite the two sides sharing 6 hydrogen bonds, they vary greatly in their arrangement, as the H – H' strands run adjacent to each other in an antiparallel fashion forming an almost planar surface (Figure 1.6).[3] This, however, is not as simple for the F to F' border, which has a greater distance between strands and each strand presents many planes of its peptides at right angles towards the other strand.[3] Due to this peculiar arrangement the F to F' bonds utilize well defined water molecules between the V94 and H90 positions as well as a bond between the two carbonyl oxygens of the mirrored E92 positions and require the E89 to V94 positions to bond with their main chain (Figure 1.6).[3] Tetrameric TTR is formed through two dimers interacting at their AB and GH loop regions.[3] The strength and propensity in which TTR monomers form their dimeric conglomerates has led to the belief that the dimeric version of TTR is in fact the basic unit of the molecule, rather than the monomer.[3] A hydrophobic pocket is developed at the center of the protein after conformation of

the dimers into a tetramer, allowing a thyroxine molecule to dock on either side of the pocket while holo-RBP is able to bind to pockets created through AB loop interactions that are perpendicular to and not overlapping the main hydrophobic core (Figure 1.4a & 1.4b).[3]

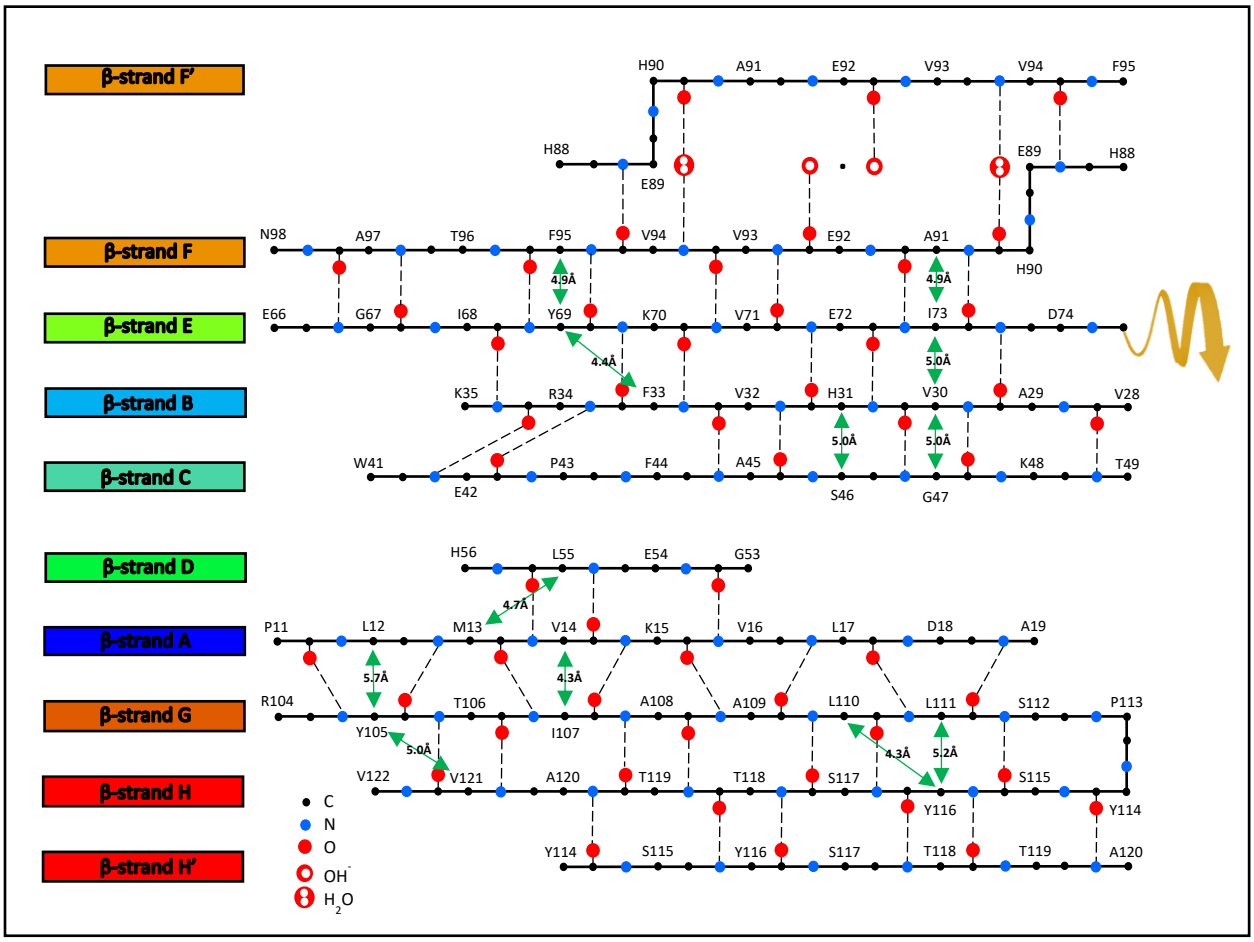

Figure 1.6 Hydrogen bond locations between β-strands of β-sheets CBEF and DAGH with internuclear distances determined by a selective labeling scheme propagating isolated ^{13}CO-$^{13}C\alpha$ dipolar-coupled spin pairs for solid-state NMR experiments.[3,17] Monomer-monomer interface hydrogen bonds are shown as F to F' and H to H', illustrating β-strands of bound monomers FEBC-DAGH and F'E'B'C'-D'A'G'H' in the TTR dimer.[3]

1.4 TTR Amyloid Aggregation Pathways

The genesis of amyloidosis involving TTR arises first from dissociation of the protein while it is in its native tetrameric state.[2,9] This tetrameric deterioration is the rate-limiting step in the dissociation of native TTR into amyloidogenic species and is theoretically capable of undergoing three unique pathways of dissociation.[9] The first of such pathways takes into consideration that monomers are the primary subunit of the quaternary structure, leading to sequential dissociation of individual monomers directly from the tetramer.[9,23] The other two pathways involve formation of dimeric forms of TTR through breaking either the AB-A'B' and symmetrically disposed GH-G'H' loop interactions or H-H' and F-F' β-strand bonds (Figure 1.7).[9,23,26] In order to bypass the rate-limiting step of tetrameric dissociation and focus solely on the mechanisms of amyloidosis, studies were performed on monomeric TTR (m-TTR) incubated under acidic conditions to aid in accelerating aggregation rates.[11,23,26] It was found that the aggregation kinetics of m-TTR follows a downhill polymerization model, where each step has a first-order monomer concentration dependence and is essentially irreversible.[11] After dissociation of the native tetramer into symmetrical dimer pairs, the dimeric interface of monomers along the F to F' and H to H' β-strands further degenerates the dimer into its native monomers (Figure 1.7).[9,23,26] Once the monomers have fully distinguished themselves, they undergo a downhill polymerization beginning with conformational changes in the AB loop region causing an unfolding into globular structures consisting of mainly β-sheets that exist in an aggregate prone state (Figure 1.8).[6,9,23] This study's hypothesis proposes that while the AB loops and connecting β-strands are marginally destabilized by their monomers structural changes, the H-F β-strand interfaces remain largely intact, allowing them to mutually bond with symmetrically mirrored aggregate prone monomers, leading to the formation of a slightly more stabilized misfolded dimeric state (Figure 1.8).[6,7] These aggregate prone dimeric species are then capable of bonding with similar species through interactions between loop regions which in turn form larger hexameric species that

have been found to be the foundation of larger aggregate formations, including cytotoxic oligomers and amyloid protofibrils (Figure 1.8).[6,7,17] Amyloid fibrils formed in this fashion from full-length TTR monomers have been categorized as Type B fibrils, which have been found to be accompanied by Type A fibrils consisting of a shortened residue fragment, 49-127, which has been proteolytically cleaved at the Lys48-Thr49 peptide bond.[18] These cleaved fibrils arise from an alternate aggregation pathway to that of Type B fibrils and have been observed in vivo of patients suffering from a more aggressive, early onset and fatal systemic amyloidosis brought on by a unique S52P mutation of TTR.[18] The exact mechanism in which these fibrils are being cleaved is unknown, however, due to the high specificity of the peptide cleavage it is thought to be a serine protease similar to trypsin.[18] Previous studies on Type A fibrils have shown they consist of large proportions of truncated fibrils not found in Type B fibrils.[18] Type A fibrils have been shown to demonstrate increased aggregation kinetics, forming cytotoxic oligomers believed to be largely responsible for the diseases underlying pathology.[5,7]

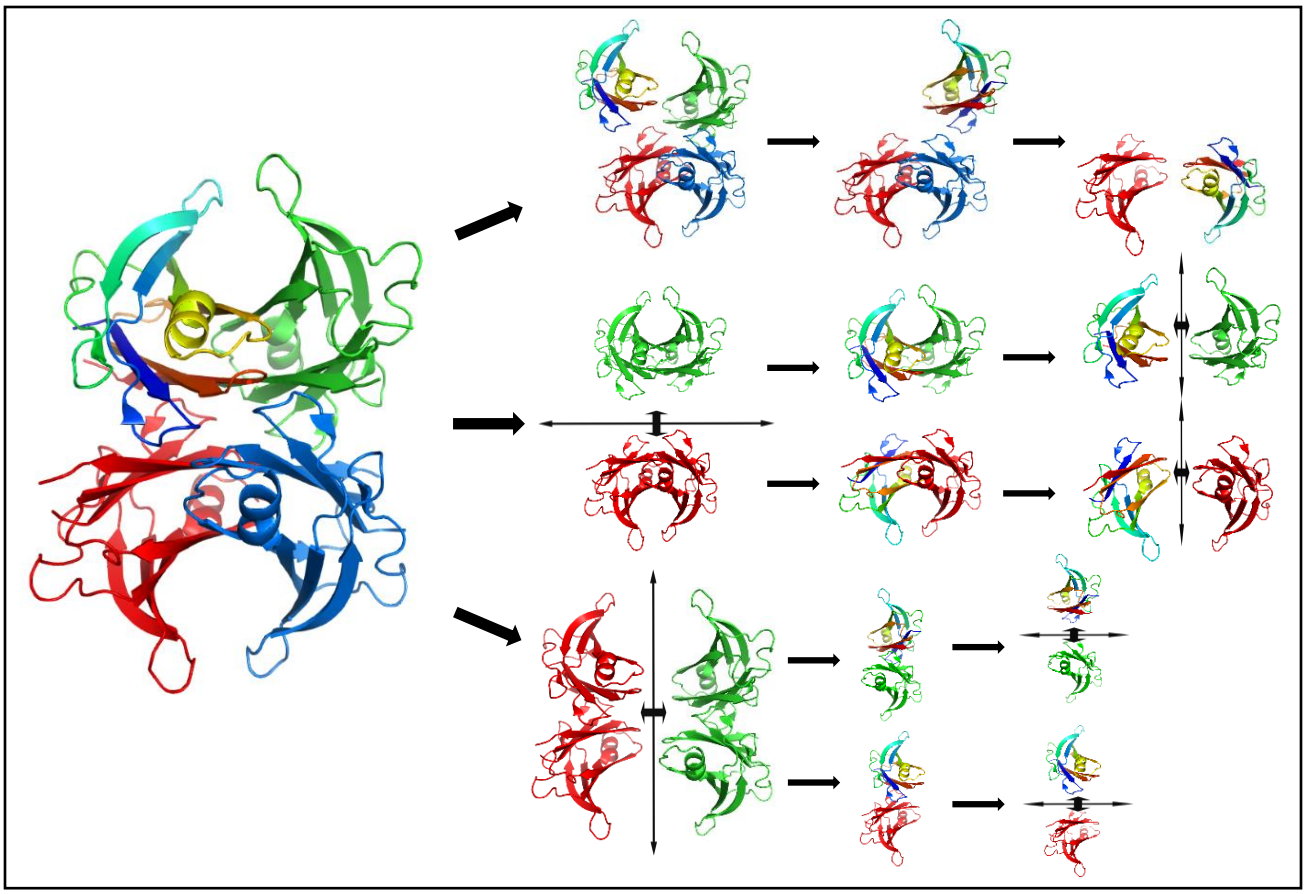

Figure 1.7 Possible dissociation pathways for TTR's native tetrameric state.

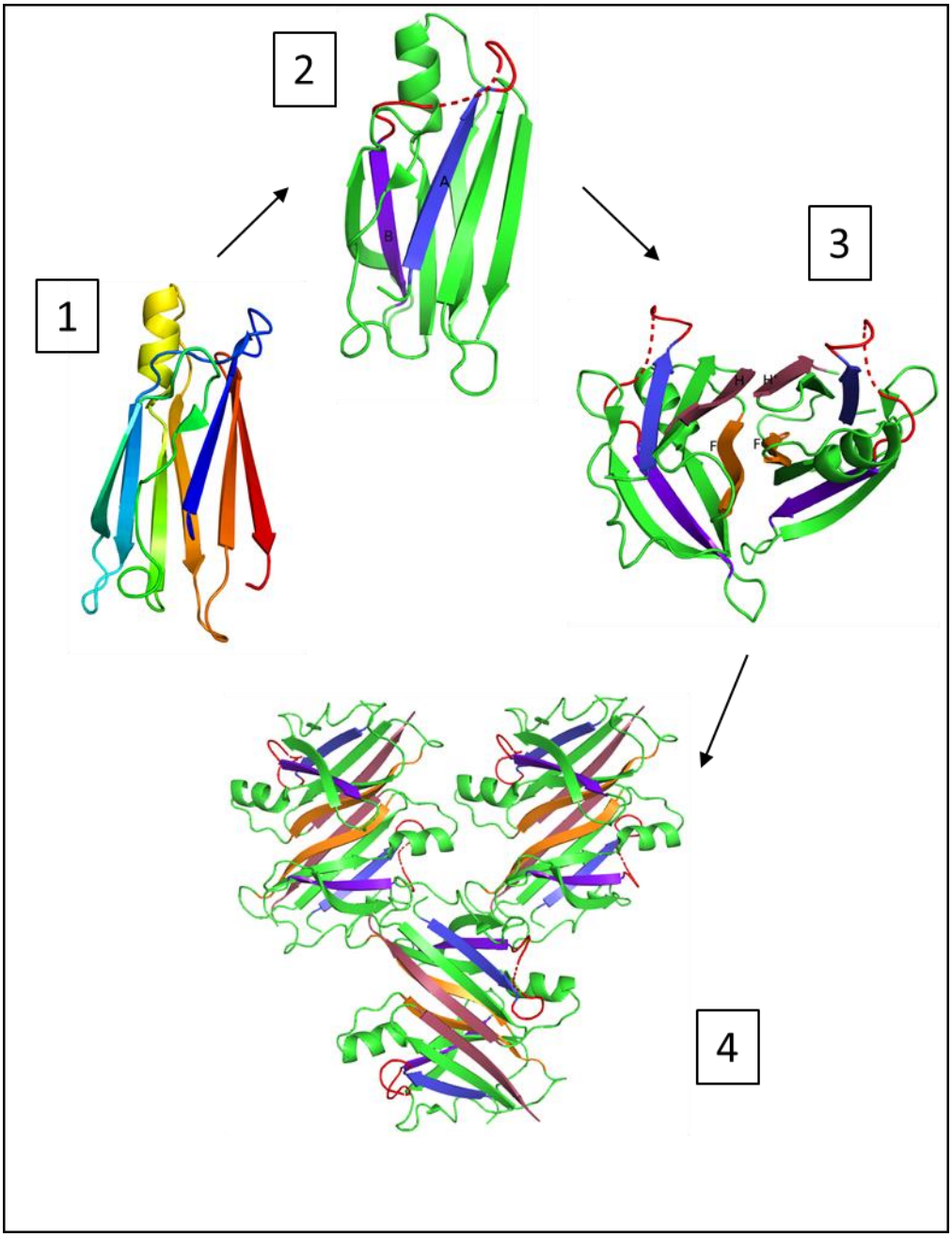

Figure 1.8 Proposed aggregation pathway for hexameric intermediaries known to be precursors to small fibrillar and large annular oligomers in-vitro.

As previously mentioned, amyloid fibril formation is a nucleation driven process which depends heavily on the propensity of steric zippers to interdigitate into the main structural β-sheets that form the cross-β spines.[23,24] In order to elucidate the segments of the TTR monomer which may be amyloidogenic, structural-based computational analysis using tools like ZipperDB have been previously performed on various segments in TTR which may have a propensity for forming steric zippers. In one such study, eight possible segments where found which have high likelihoods of aggregating with structures of similar peptide sequences through steric zippers (Figure 1.9).[23]

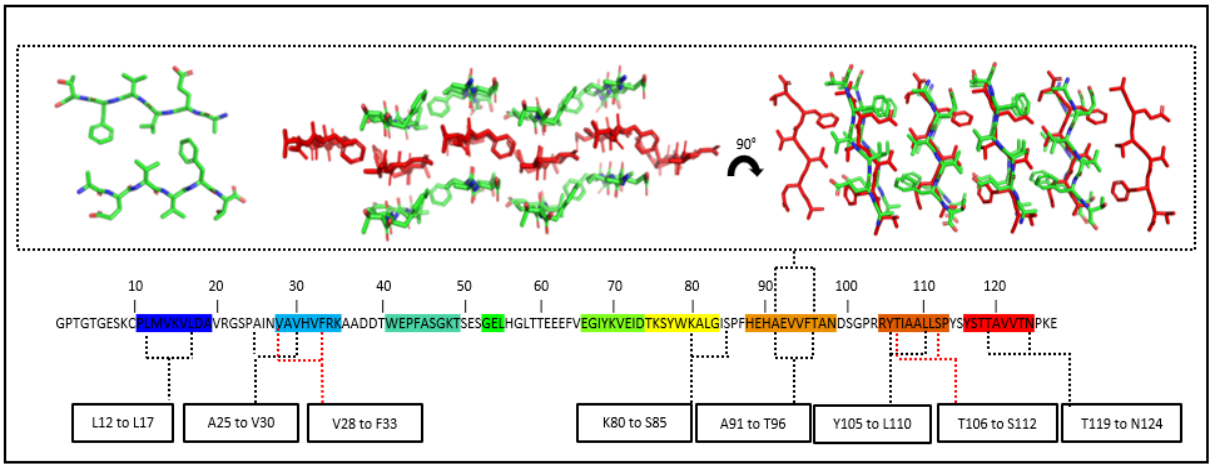

Figure 1.9 Structural based computational analysis on the TTR monomer showed 8 possible sites associated with the ability to create steric zippers typically seen in amyloid fibril formation. The planar symmetry of section A91 to T96 is illustrated (top left), showing the tightly packed anti-parallel boundary shared between two copies of itself. How this translates into a Class 7 up-up anti-parallel steric zipper formation is illustrated (top middle and right).[7]

Proline substitutions, which have been shown to inhibit amyloid formation in TTR, were then performed on the segments thought to be involved in steric zipper formation.[12] Substitutions S85P, E92P, V94P and the double substitution S85P/E92P all altered the morphology of aggregates and greatly reduced aggregation kinetics.[12,23] In an isolated segment of WT-TTR's F-strand (A91 to T96), introduction of the E92P substitution completely inhibited fibril formation, and crystallographic structural analysis of this segment after incubation showed exposed β-sheets layered in an anti-parallel β-sheet formation, leading to the hypothesis that this segment and the N-terminally adjacent region may be integral parts of the amyloid aggregation pathway.[23,24] A majority of the fibril core of the TTR amyloid is made up of large portions of the protein, suggesting there may be more than one amyloidogenic site.[9,23,26] Since monomeric TTR is much more amyloidogenic than tetrameric TTR and the F strand is buried within the tetramer yet exposed in the monomer, it was reasoned that other fibril forming segments may be found by looking at their exposed surface area to solvents in the tetramer versus monomer.[23] The peptide sequence T119 to N124 in the H strand were then found to meet the computational standards for steric zipper formation and to have a similar relationship with solvent exposure as the A91 to T96 segment.[23] When substitutions were done with a bulky molecule, such as tryptophan, for a short chain amino acid such as threonine or valine within the peptide backbone, it was found that incubated segments containing the T119W and V121W varieties produced no aggregates after 4 days.[23] The larger molecules were found necessary for successfully preventing the tightly packed steric zipper formation necessary for amyloid formation due to similar proline substitutions being ineffective for this strand.[23]

Given what has been found about the aggregation of misfolded dimers, as well as the ability of peptide sequences located within the F and H β-strands to aggregate into oligomers and their propensity to form steric zippers necessary for amyloid formation, it was determined that the goal of this study would be to examine the effects of sterically hindering

mutations introduced into the F and H-strands of the native state as well as the monomeric state of TTR in order to gain further insights into the molecular mechanisms linking the dimerization of misfolded TTR monomers and ATTR.

1.5 Research Goals

Given what is currently known of the mechanisms behind ATTR, the goals of this research are to demonstrate an ability to either greatly slow or completely inhibit the oligomerization process of ATTR through destabilization of the F-F' to H-H' dimeric interfaces. First, aggregation kinetics will be monitored for WT-TTR under acidic as well as physiological conditions to observe the structural changes over time and the rate at which aggregation occurs. As proteolytically cleaved C-terminal fragments have also been found circulating in-vivo of ATTR patients, samples prepared at a neutral pH were proteolytically cleaved through trypsin digestion. These observations were aimed towards confirming previous studies performed on the ability of WT-TTR to form amyloidogenic species, specifically focusing on the dimerization phase of aggregation as well as the rate at which these species arise. In tandem with the wild type studies, analytical structural and kinetic based analysis will be performed on two of the most amyloidogenic species of TTR, L55P and V30M, providing insight into any reliance upon dimerization they may share with WT-TTR with regards to the oligomerization process. The hypothesis of this thesis expects to see a pattern in which the native TTR tetramer dissociates first into its monomeric form with small concentrations of dimers, followed by increased dimeric formation in subsequent days and eventually the formation of oligomeric species. This pattern would indicate that the ability of TTR to form dimers upon aggregation is fairly significant in regard to its overall oligomerization. In order to further probe the importance of the dimerization step, mutations T119W and E92P will be introduced into the native protein, both of which are large sterically hindering amino acids, which inhibit their associated β-strands ability to form the closely packed hydrogen bonds necessary for monomer interface coupling. The ability of these two

mutants will be further scrutinized by transforming them into L55P-TTR, ideally demonstrating their capability to inhibit dimer formation, and thus any subsequent oligomer formation, in even one of the most highly amyloidogenic species of TTR. As the E92P and T119W mutations will be introduced into the native tetrameric state of WT-TTR and L55P-TTR, leading to the possibility of them affecting the dissociation process of TTR and subsequently its oligomerization, an aggregate prone TTR variation with mutations introduced at the F87M and L110M positions will be examined as well. This species of TTR has been shown to quickly dissociate into m-TTR, making it an ideal candidate to study the initial dimerization and following oligomerization of TTR as it aggregates. Once the structural profile of aggregating m-TTR has been confirmed, the inhibitory effects of the E92P and T119W mutations may be focused on solely in the realm of how they affect the aggregation process of misfolded TTR monomers. Upon completion, these studies are designed to demonstrate that the formation of oligomeric species of TTR are highly dependent upon the integrity of the F-F' to H-H' dimeric interfaces found within the active binding site of two identically misfolded monomers undergoing aggregation. This revelation may help the development of future gene-based therapeutical strategies focused on the prevention or suppression of amyloidogenic TTR species found in-vivo.

Chapter 2: Methods and Materials

2.1 Protein Expression and Purification

In preparation for these steps, 3 L of LB medium was split evenly into six 2.8 L Erlenmeyer flasks and from these, a total of 200 mL was evenly syphoned into four 250 mL Erlenmeyer flasks. All flasks were then covered and autoclaved under steam at 15 psia and 121 °C for 40 minutes. All materials were allowed to cool to room temperature before proceeding.

All TTR plasmids were transformed into a calcium competent strain of *E. coli* as follows:

1. A 100 µL sample of *E. coli* strain BL21(DE3) was removed from -80 °C storage and left to thaw in ice for 5 minutes.
2. A 10 µL sample of a pHMMA plasmid encoded with either WT, L55P, or m-TTR was removed from -20 °C storage and left to thaw in ice for 5 minutes.
3. Once thawed, 1 µL of the plasmid was pipetted into a prechilled sterile culture tube followed by 10 µL of *E. coli* directly on top of the plasmid.
4. This culture tube was then placed in ice and left to incubate for 20 minutes.
5. During incubation, a hot water bath is prepared and brought up to 42 °C.
6. After 20 minutes, the culture tube is submerged in the hot water bath for 30 seconds and immediately returned to the ice for 2 minutes.

All TTR variants were plated onto LB agar plates containing carbenicillin as follows:

7. Following completion of the transformation, 800 µL of sterile LB medium was pipetted into the culture tube.
8. This solution was placed inside a 37 °C incubator and left to shake at 250 RPM for 1 hour.
9. After 1 hour, 80 µL of this solution was then plated onto a LB agar plate prepared with carbenicillin prewarmed to approximately 37 °C.

10. The plate was then left in a stationary 37 °C incubator for approximately 12 hours or until sufficient colony growth was observed. This study was careful to avoid overexpression during this phase.

All TTR variants were expressed into 3 L cultures as follows:

11. To prepare for expression, 5 mL of LB medium was carefully pipetted from each of the 250 mL Erlenmeyer flasks prepared previously into four sterile culture tubes. 5 µL of carbenicillin was then mixed into each culture tube containing 5 mL of LB medium.
12. Four single, medium sized, colonies were chosen and, using a sterile inoculating loop, each colony was lifted and mixed into their respective tube. All tubes were then incubated at 37 °C while shaking at 250 RPM for 2 hours.
13. After incubation of the 5 mL cultures is complete, each tube's contents were then transferred back into their former 250 mL flask and 50 µL of carbenicillin was added. The four 250 mL flasks were then shaken at 250 RPM and 37 °C for 3 hours.
14. Once expression of the 200 mL culture was complete in the 250 mL flasks, they were then combined and evenly redistributed amongst the six 2.8 L Erlenmeyer flasks. 500 µL of carbenicillin was then added to each flask and all flasks were left to incubate at 37 °C and shaking at 250 RPM for approximately 2 to 3 hours.
15. At the 2 hour mark, a 1 mL aliquot was obtained from each 500 mL culture to measure the OD at 600nm. Once the OD_{600} of each flask's culture was found to be between 0.6 and 0.8, they were simultaneously induced with 1 mL of 1,000 times concentrated IPTG. The flasks were then incubated at 25 °C while shaking at 250 RPM for approximately 14 hours.
16. After approximately 14 hours, the OD_{600} was obtained again for each 500 mL culture to ensure readings were between 1.5 and 1.6. Upon reaching the desired OD_{600}

range, cells were harvested in six 250 mL Nalgene bottles via centrifuge at 8,000 RPM.

17. The six Nalgene bottles with bacterial pellets were then placed in a -80 °C freezer for a minimum of 1 hour.

All TTR variants were purified via the following process:

18. All six Nalgene bottles were retrieved from the -80 °C storage and allowed to thaw for approximately 30 minutes on ice.
19. 300 mL of a cold 1M Tris buffer with 5M NaCl lysing solution was evenly distributed into each Nalgene bottle. The bacterial pellets were then completely resuspended.
20. The contents of each bottle were then mixed into a clean metal cup on ice. The sonicator probe was then lowered into the cup sitting in ice and the solution was sonicated for five 1-minute cycles at an amplification of 50% and pulse intervals of 30 seconds. A two minute break was taken between each cycle to allow the solution to completely cool.
21. The lysed solution was then evenly distributed into two 250 mL Nalgene bottles and centrifuged for 30 minutes at 8,000 RPM and 4 °C.
22. After centrifuging, the supernatant was removed from each bottle and recombined in a cold glass beaker.
23. Using 90.32 grams of ammonium sulfate was determined to bring the approximately 300 mL of lysed solution at 4 °C up to a 50% ammonium sulfate saturation level. The ammonium sulfate was added slowly to the solution while stirring at 4 °C. For 300 mL of m-TTR at 4 °C, 41.82 grams were added for a 25% ammonium sulfate saturation level.
24. Upon complete homogenization, the salted solution was then even distributed into two 250 mL Nalgene bottles and centrifuged for 30 minutes at 8,000 RPM and 4 °C.

25. The supernatant was collected from each Nalgene bottle and combined in preparation for dialysis.
26. A total of 8 L of dialysis buffer was prepared using 1M Tris, 0.5M EDTA, PMSF and deionized water. It was then separated evenly into four 3 L containers. PMSF was added just before the dialysis bags were ready to be placed into the dialysis buffer due to its instability in water.
27. Using 6-8 kDa dialysis bags (3-5 kDa bags for m-TTR), the salted and lysed protein solution was evenly distributed and clipped using weighted bottoms.
28. The dialysis bags were then split into two dialysis buffer buckets, each containing 2 L of dialysis buffer. A magnetic stir bar was placed in each bucket, and they were then placed in a cold room on stir plates to let spin for 6 hours.
29. After 6 hours, the remaining two precooled dialysis buffer buckets were brought into the cold room and the dialysis bags were swapped over into the fresh buffer to spin for another 10 hours.
30. With dialysis complete, the desalted solution was collected from each bag into a single chilled glass beaker on ice.
31. This solution was then loaded in a 10 mL HiTrap™ Q HP (GE Healthcare) AEC, which had been previously washed with Buffer A (20mM Tris, pH 8.0).
32. Four washes were then performed on the column using a 5% gradient increase in Buffer B (20mM Tris, 5M NaCl, pH 8.0) flowthrough.
33. A preset method in the software was then used to gradually increase the amount of Buffer B being introduced into the column in order to elute the protein.
34. The software provided produced an AEC profile curve (saved locally onto the hard drive) which indicated where the most desirable Q fractions were. Each fraction came off of the column in 2 mL samples that were collected into clean disposable glass culture tubes. These 2 mL samples were then evenly split into two 1 mL

microcentrifuge tubes and, using liquid nitrogen, flash frozen to then be stored in a -80 °C freezer.

35. In order to obtain soluble forms of the protein for experimentation, each Q fraction is then injected into a HiLoad© 16/60 Superdex 200 gel SEC and eluted using PBS buffer (0.2M monosodium phosphate, 0.2M disodium phosphate, pH 7.4).
36. UV spectroscopy was then used to check the concentration of the collected protein using a 1 mm quartz cuvette at a wavelength of 280nm and a previously determined extinction coefficient of 7.76×10^4 M^{-1} cm^{-1}.
37. Once the concentration of the pooled purified gel fractions was known, in order to achieve the desired experimental concentration, the solution was either diluted using pH 7.4 PBS buffer or it was concentrated further using 10 kDa centrifugal filter.

2.2 Protein Sample Preparation

1. For studies performed at a pH of 4.4, protein concentrations were raised to 2.0 mg/mL through centrifugation and diluted at a volumetric ratio of 1:10, protein to 10 mM acetic acid buffer solution, achieving an effective protein concentration of 0.2 mg/mL. Samples prepared for aggregation kinetic studies were done so at room temperature, whereas samples prepared for SEC structural characterization profiles were all prepared in a cold room at 4 °C.
2. For proteolytic cleavage, samples were incubated with trypsin at a concentration ratio of 1:100 trypsin to protein.

2.3 Site Directed Mutagenesis

Invitrogen ™, Phusion ™ Site-Directed Mutagenesis Kit purchased from Thermo Fisher Scientific.

1. A polymerase chain reaction (PCR) mixture was prepared according to instructions provided in the mutagenesis kit. In a microcentrifuge tube, 10 μL of “5x Phusion HF Buffer” was first added, followed by; 1 μL of “10 mM dNTPs”, 0.25 μL of “Forward primer”, 0.25 μL of “Reverse primer”, 10 ng of template DNA, and 0.5 μL of Phusion Hot Start DNA Polymerase (2 U/μL). The mixture was diluted to 50 μL using “PCR H_2O” and mixed gently using a pipette.
2. The PCR mixture was then placed into a programmable thermo-cycler. Initial denaturation took place at 98 °C for 30 seconds. Next, 25 cycles of denaturation, annealing and extension took place at 98 °C for 7 seconds, 65 °C for 20 seconds, and 72 °C for 20 seconds respectively. A final extension was performed at 72 °C for 5 minutes with a final hold set for 4 °C.
3. After thermocycling, the PCR mixture was subjugated to a ligation reaction by first introducing 1 μL of “FastDigest DpnI enzyme” and incubating at 37 °C for 15 minutes. After DpnI digestion, a 10 μL ligation reaction mixture was prepared in a microcentrifuge tube by first taking 3 μL of PCR mix and adding 2 μL of “5x Rapid Ligation Buffer”, 4.5 μL of “PCR H_2O”, and 0.5 μL of T4 DNA Ligase, then mixed well. This mixture was briefly centrifuged then allowed to incubate at room temperature, approximately 25 °C, for 5 minutes and placed on ice in preparation of transformation into competent *E. coli* cells.

2.4 UV Spectroscopy for Aggregation Kinetics Analysis

1. For kinetics studies involving O.D. readings, 1 mL aliquots of purified protein at a desired concentration were sterile filtered into disposable UV spectroscopy cuvettes.
2. The tops of the cuvettes were then wrapped in parafilm, and they were allowed to incubate at 37 °C while shaking at 250 RPM.
3. These cuvettes were periodically measured using UV spectrophotometry at a wavelength of 400 nm.

2.5 Size Exclusion Chromatography (SEC)

SEC profiles were obtained for oligomerization studies during the course of sample incubation.

1. Approximately 600 µL of solution was taken into a syringe and filtered through a 0.2 µm sterile filter tip.
2. From the filtered solution, 500 µL was injected into the FPLC (GE Healthcare) which was connected to a Superdex© 200 10/300 GL SEC.
3. SEC profiles were saved locally to an in-lab computer and exported for data analysis.

Chapter 3: Results

3.1 WT-TTR aggregation involves dissociation into monomeric species followed by aggregation into dimeric and oligomeric species

To gain structural insight into the steps associated with the aggregation of misfolded TTR, aliquots of TTR incubated at 0.2 mg/mL under acidic conditions (pH 4.4 at 4 °C) were injected into a size exclusion gel chromatography column (SEC) daily over a week for observations (Figure 3.1). Acidic conditions have been previously shown to be necessary to enhance the aggregation process of TTR as it remains fairly stable at neutral pH.[9] Injections performed prior to incubation (Figure 3.1, Day 0) indicated a majority of the protein present was in its native tetrameric state. Over the course of the next two days, the tetrameric fractions have decreased, giving rise to a significant quantity of monomeric species and smaller amounts of dimeric species (Figure 3.1, Day 1 & Day 2). On Day 3, the concentration of dimeric species continues to rise as the monomeric species remains constant and the tetrameric species continue to decrease (Figure 3.1, Day 3). This observation indicates that the direction of aggregation is moving from tetramer to monomer leading into a reformation of a dimeric species following the initial dissociation. After a week of incubating, the samples collected were observed to have had a majority of their dimeric species convert into high molecular weight oligomeric species while the overall amount of monomeric remains seemingly in equilibrium with the process as its levels remain constant even as the tetrameric species continue to decrease (Figure 3.1, Day 7).

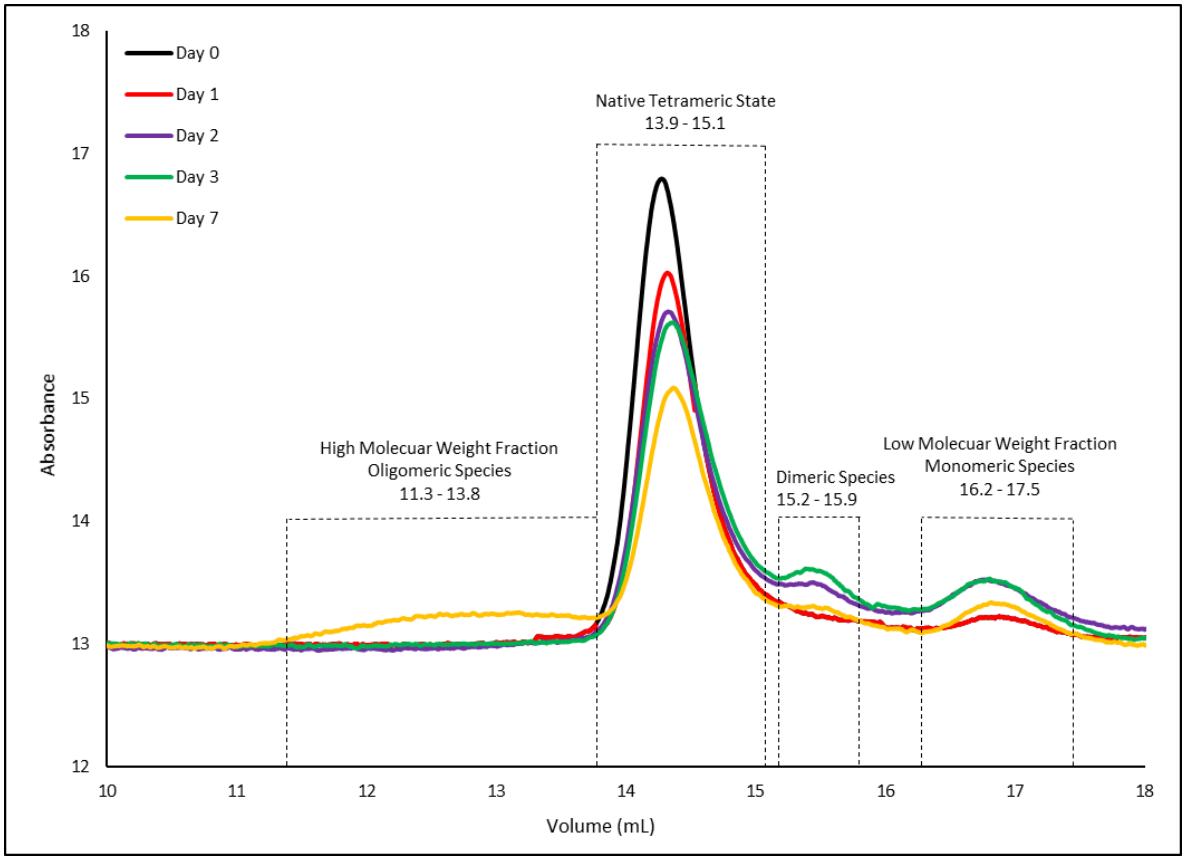

Figure 3.1 SEC profile of WT-TTR incubated at 0.2 mg/mL, a pH of 4.4, and at 4 °C for seven days.

3.2 Highly amyloidogenic species, V30M-TTR and L55P-TTR, follow an accelerated aggregation pathway similar to that of WT-TTR

In order to establish if there is a pattern between the aggregation pathways of WT-TTR and those of mutated species commonly associated with hATTR, the highly amyloidogenic V30M and L55P mutations were introduced into native TTR and incubated under identical physiological and environmental conditions to the initial WT-TTR study. V30M-TTR showed similar aggregation characteristics to that of WT-TTR, with its initial injection revealing a large tetrameric peak (Figure 3.2, Day 0), and subsequent injections showing increased monomeric and dimeric concentrations. However, tetrameric dissociation appears to be accelerated after

only a day of incubation, leading to a much lower concentration of tetrameric species after one day in comparison to WT-TTR. These lower tetramer concentrations are also accompanied by substantial monomer and dimer concentration, indicating that the aggregation process is more accelerated than that of WT-TTR (Figure 3.2, Day 1). The Day 2 and 3 profiles indicate that the aggregation process proceeds to follow that of WT-TTR, where it continues to dissociate its native tetramer into monomers, these monomers remain at a constant concentration in equilibrium, leading instead to further development of dimeric species. After a week of incubation, the native tetramers have been nearly totally dissociated, with the concentrations of dimers also being diminished, giving rise to large concentration of high molecular weight oligomers (Figure 3.2, Day 7).

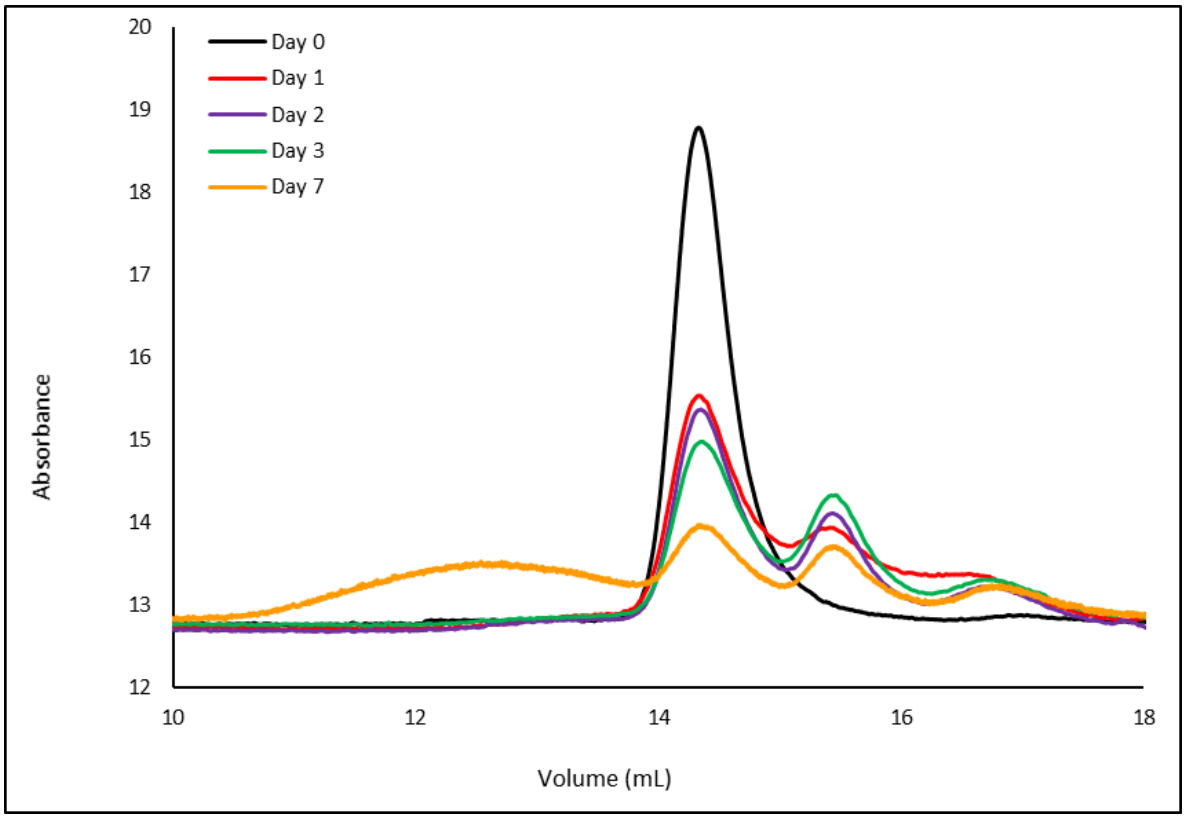

Figure 3.2 SEC profile of V30M-TTR incubated at 0.2 mg/mL, a pH of 4.4, and at 4 °C for seven days.

Analysis of L55P-TTR SEC profiles indicate a similar aggregation pattern to that of WT-TTR and V30M-TTR, with an even greater increase in aggregation kinetics than that of V30M. Initial injections, performed immediately after sterile filtration of protein samples prior to incubation, showed decreased native tetramer concentrations than those of the initial injections for both WT and V30M (Figure 3.3, Day 0). These decreased tetramer concentrations are also accompanied by the presence of monomeric and dimeric species. This observation indicates that L55P-TTR undergoes immediate dissociation and aggregation upon entering highly acidic environmental conditions. Outside of this initial difference, the aggregation profile continued to reflect those of the WT and V30M studies, where an increase in dimeric species is observed over the first few days with a large rise in oligomeric species after a week (Figure 3.3 Days 2, 3, & 7).

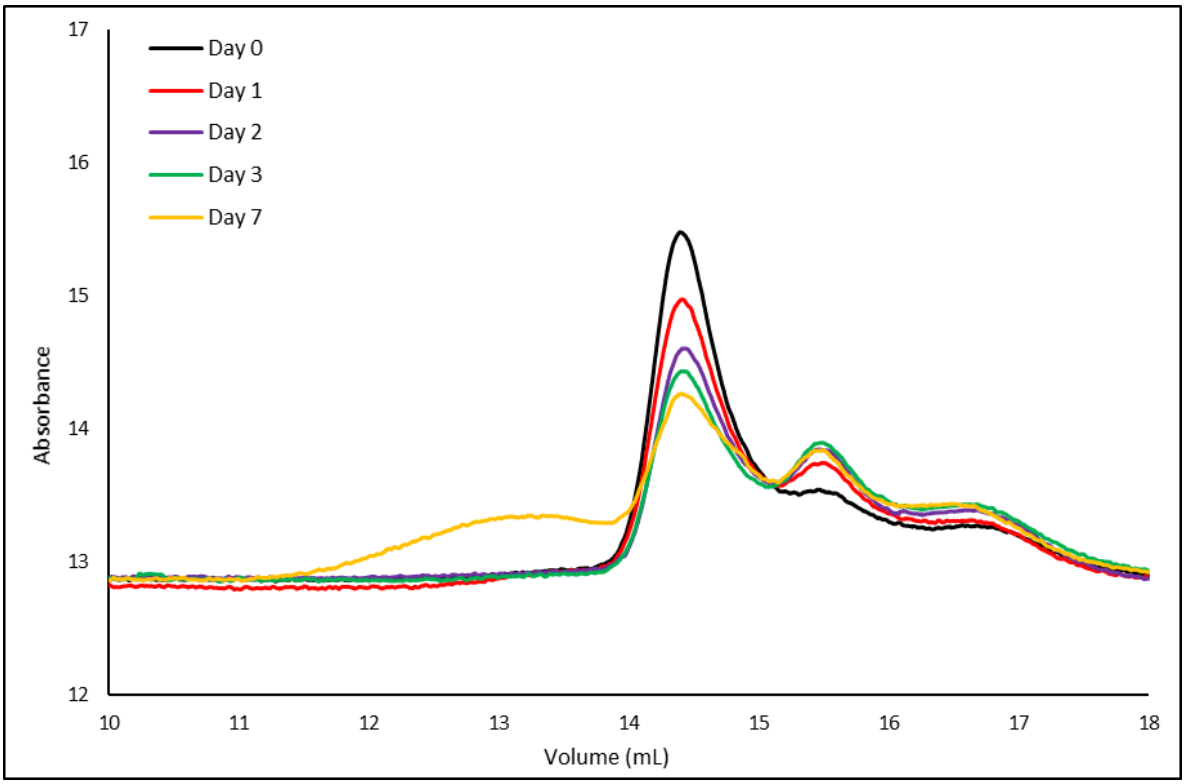

Figure 3.3 SEC profile of L55P-TTR incubated at 0.2 mg/mL, a pH of 4.4, and at 4 °C for seven days.

3.3 Mutations T119W of the H-strand and E92P of the F-strand inhibit the aggregation of WT-TTR oligomers by blocking the formation of the intermediate dimeric state

As both the dissociation and amyloid aggregation pathway involve misfolded monomers transitioning through dimeric states, it was determined that introduction of bulky amino acid sidechains into one of the two possible dimeric interfaces within TTR should be observed to see how the aggregation kinetics respond. To first probe the effects of destabilization of the H to H' β-sheet interface, a tryptophan mutation was introduced at the T119 position of WT-TTR. Due to the large size of the tryptophan compared to that of threonine, the tightly interdigitated H to H' β-strand bonds are unable to form, leading to a theoretical halt in the oligomerization process. In order to induce immediate aggregation, studies were first performed at a pH of 4.4 while shaking at 250 RPM and 37°C (Figure 3.4, top). Optical density readings at a wavelength of 400 nm were then taken over the course of 64 hours to observe any changes in oligomeric species. It was found that the introduction of the bulky tryptophan molecule in the mutated species caused a clear reduction in the aggregation kinetics of the native state tetramer at these physiological conditions, observable by both the decreased rate at which they aggregate as well as their overall absorbance. Previous studies have found fragmented TTR in heart biopsies of FAP patients predominantly comprised of the peptide strands T49 to E127, known as Type A fibrils.[18] To investigate the effects of the T119W mutation upon these Type A fibrils, proteolytic cleavage of the peptide bond K48 to T49 in the CD loop was induced via trypsin digestion. It was found in this study that the T119W mutation reduced the aggregation of the Type A fibrils nearly completely compared to identically prepared cleaved reference samples of WT-TTR (Figure 3.4, bottom).

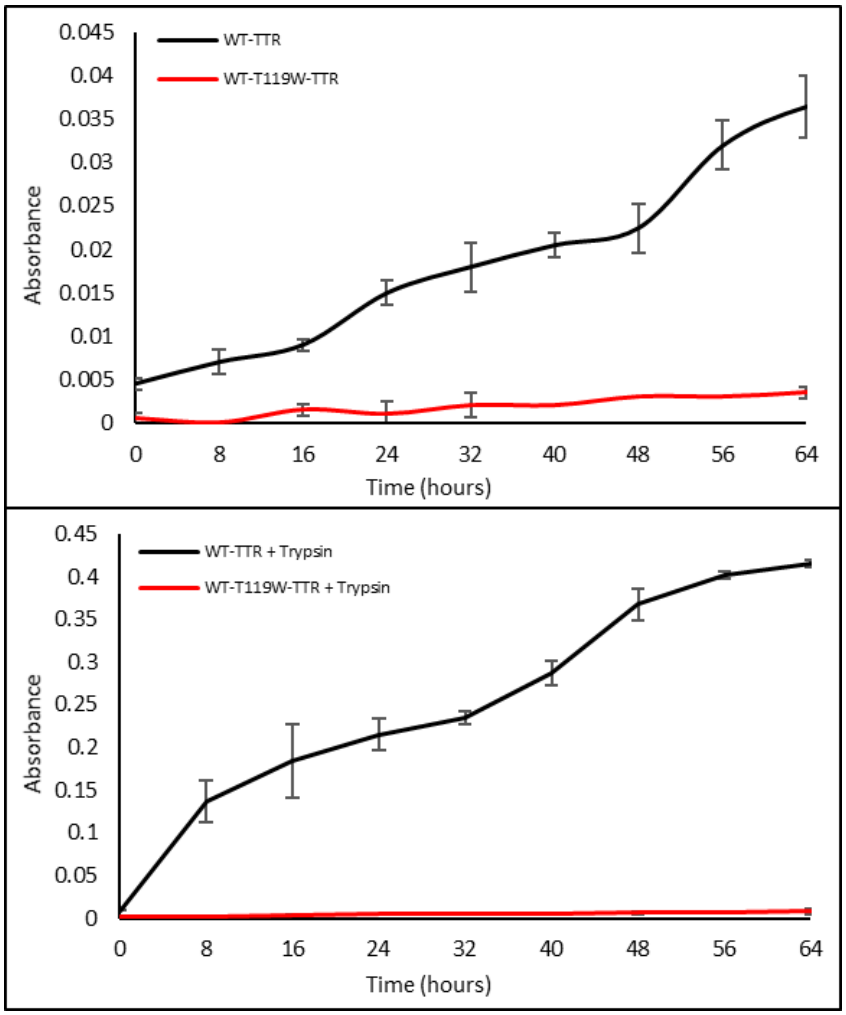

Figure 3.4 Aggregation kinetics observed at an OD_{400} of WT-TTR with the T119W mutation at 37 °C. Samples incubated at a pH of 4.4 with shaking (top). Samples incubated at a pH of 7.4 with trypsin while shaking (bottom).

An identical set of studies were next performed focusing on the apparent relevance of the F to F' β-strand interface by introducing a proline substitution into the E92 position of TTR's F β-strand. Similar to the T119W experiments, the E92P mutation resulted in a drastically reduced aggregation rate at a pH of 4.4 (Figure 3.4, top) and experienced a smaller exponential growth rate when incubated with trypsin (Figure 3.4, bottom). This data suggests that the E92P mutation in the F-strand inhibits the aggregation of both full-length and cleaved TTR. However, the aggregation kinetics (Figure 3.5) indicates that the E92P mutation completely blocks full-length TTR aggregation, while it only decreases the aggregation rate of cleaved TTR. This indicates that although the full-length TTR and the cleaved TTR aggregate via H and F strands, they have different aggregation pathways. Considering the two sets of results from both mutations and comparing their similar inhibitory effects upon the aggregation of both full-length and proteolytically cleaved sequences, a conclusion may be drawn that aggregation of oligomeric species is in fact greatly decreased through destabilization of the F-F' and H-H' interface. As these interfaces are located both within the native tetramer pre-dissociation as well as in the misfolded dimers post-dissociation, it would next be necessary to develop studies which focus solely on the aggregation of TTR's misfolded monomers into misfolded dimers. In order to achieve this, a variant of TTR which exists predominantly as a monomer, would be observed for structural analysis with and without the E92P and T119W mutations.

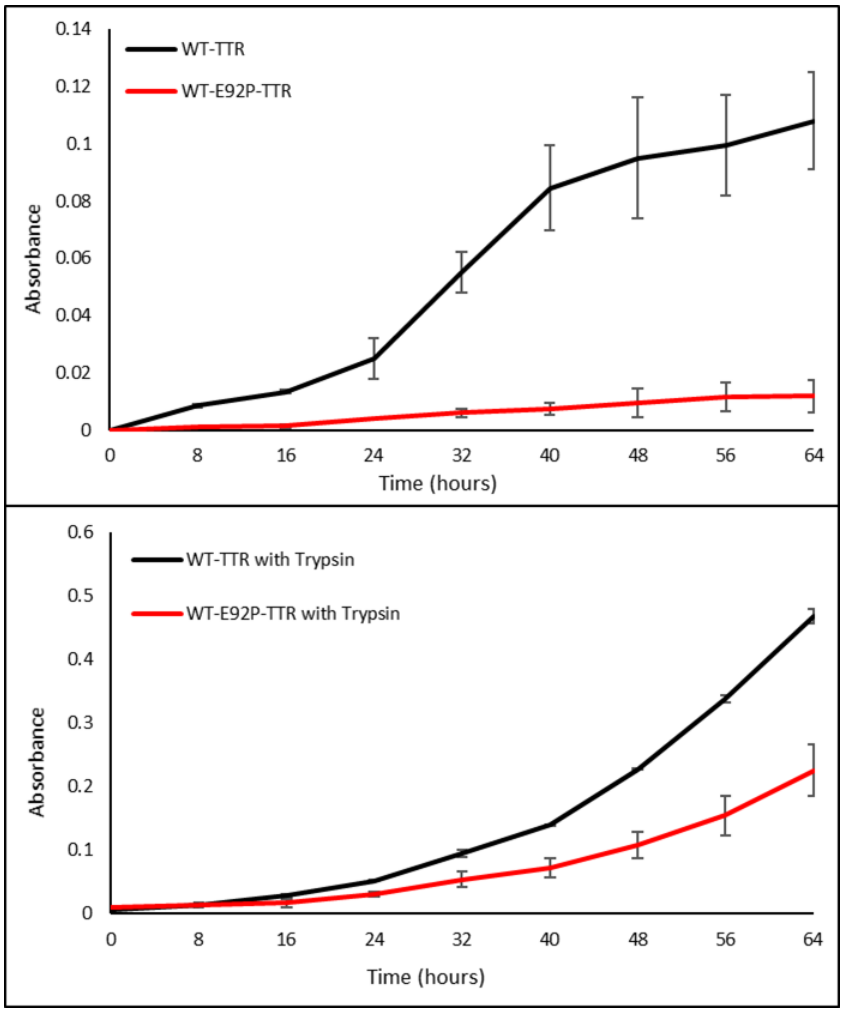

Figure 3.5 Aggregation kinetics observed at an OD_{400} of WT-TTR with the E92P mutation at 37 °C. Samples incubated at a pH of 4.4 with shaking (top). Samples incubated at a pH of 7.4 with trypsin while shaking (bottom).

3.4 Monomeric TTR reveals dimeric gatekeeping in the oligomerization process with similar responses to peptide substitutions E92P and T119W.

To eliminate one of the two possible pathways that the stabilized dimeric interface could be affecting, a mutated species of TTR (F87M-L110M) known as m-TTR, which has been previously shown to be unable to form into its native tetrameric state, was observed under identical experimental conditions as the previous native state studies.[7,11] By using this monomeric variant of TTR, the rate limiting step of tetrameric dissociation is bypassed, allowing for a focused examination of TTR's aggregation kinetics specifically.[11] As a reference for the expected behavior of m-TTR as it aggregates into oligomeric species, samples were incubated at a pH of 4.4 to induce aggregation and were then observed over the course of three days (Figure 3.6). Interestingly, the Day 0 reference injection of this variant of TTR shows the sensitive nature of m-TTR under acidic conditions to readily aggregate into small amounts of dimers and even some oligomers immediately upon denaturation (Figure 3.6). Subsequent observations demonstrated predictably similar patterns of oligomerization as compared to those of WT, L55P, and V30M TTR (Figure 3.1, 3.2, 3.3). The first of such patterns is the immediate dimerization of the monomeric constituents within the solution and as expected within 24 hours the observed monomer concentration was halved, inducing a near equal amount of dimer formation and smaller amounts of oligomer formation (Figure 3.6). During the Day 2 observations it was noted that the monomeric species in solution had not decreased at all, seemingly reaching a state of equilibrium. This monomeric equilibrium appears to drive the previous days dimeric species into continuing along the oligomerization pathway, nearly halving the total dimer concentration into a marginal increase of the overall oligomer concentration (Figure 3.6, Day 2). Interestingly, on Day 3, the dimeric species appeared to be in equilibrium as they remained constant while the monomer concentrations decreased and the oligomer concentrations greatly increased (Figure 3.6, Day 3). The study was halted after Day 3 as the

aggregation was determined to be complete due to a lack of change in the concentration of each species. After consideration of the data presented by the aggregating m-TTR species in Figure 3.6, a more concise aggregation pathway may be defined in the following order. First, the misfolded monomeric species reaches a short-lived equilibrium phase while aggregating a majority of itself into nearly equal amounts of dimers and small concentrations of oligomers. These dimeric species then appear to be the aggregation driver as they continue to form oligomeric species while the monomeric concentrations remain unchanged. The newly driving dimeric species then appear to reach a state of equilibrium in which they begin to further oligomerize while converting the remaining m-TTR into more dimers. This dimer-centric pathway of aggregation reinforces this studies hypothesis that the dimeric interface of misfolded TTR which hold these dimers together are essential in the progression of oligomerization. Now that a reference for the aggregation kinetics of m-TTR has been established, the T119W mutations were introduced, and samples were incubated under similar environmental and physiological conditions as those of WT-TTR in Figures 3.4 and 3.5 (Figure 3.7).

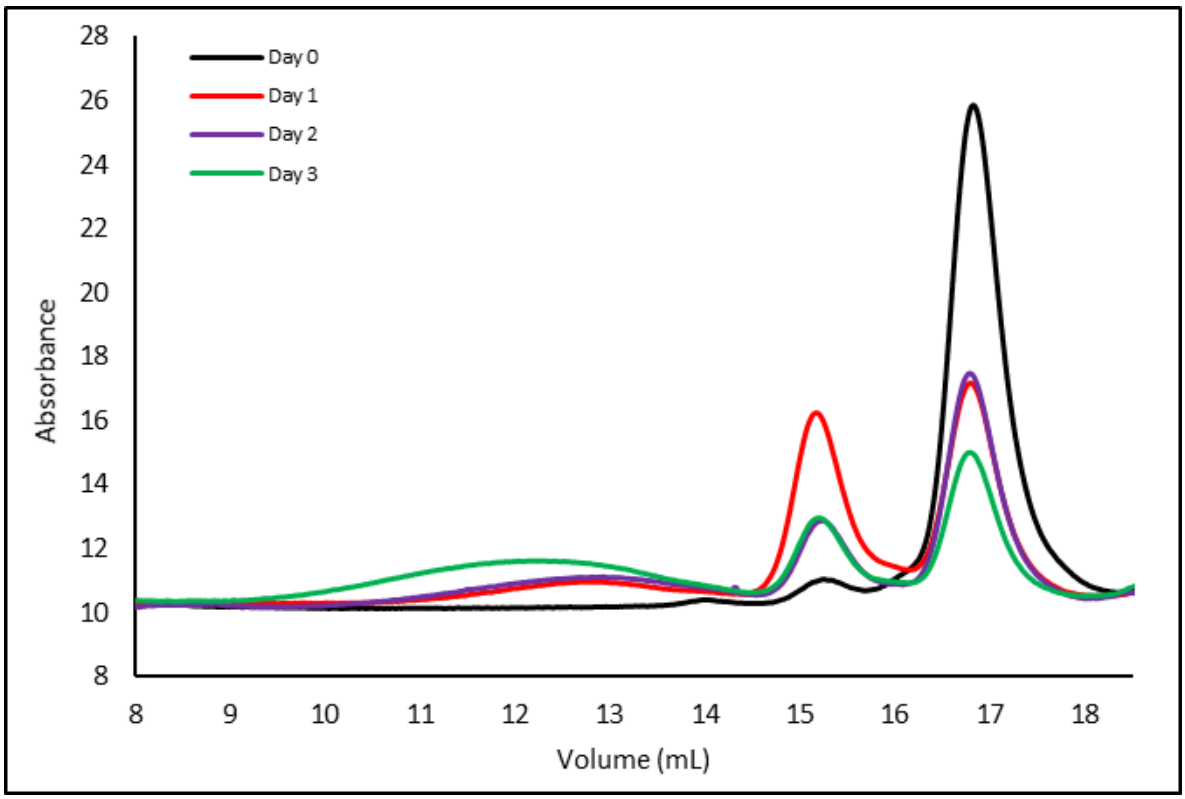

Figure 3.6 SEC profile of m-TTR incubated at 0.2 mg/mL, a pH of 4.4, and at 4 °C for three days. Monomeric conformations (16 mL – 18 mL), dimeric conformations (14.5 mL – 16.0 mL), and high molecular weight oligomeric conformations (9.0 mL – 14.5 mL) share similar elution volumes to those of WT-TTR.

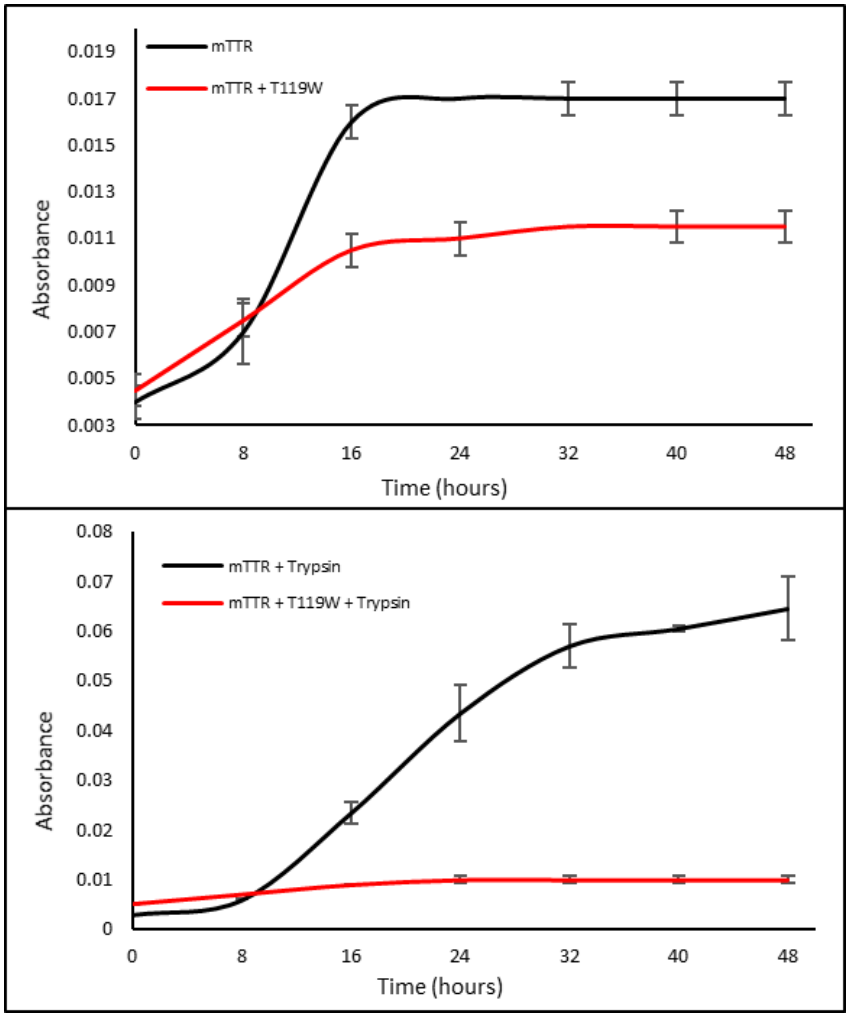

Figure 3.7 Aggregation kinetics observed at an OD_{400} of m-TTR with the T119W mutation at 37 °C. Samples incubated at a pH of 4.4 with shaking (top). Samples incubated at a pH of 7.4 with trypsin while shaking (bottom).

3.5 Introduction of the T119W mutation into the H-strand of m-TTR inhibits dimerization during the aggregation process and blocks oligomer formation

With the more well-defined aggregation pathway defined as well as having demonstrated the stabilizing effects of the T119W mutation upon the H β-strand in the native state, further examination may be performed into which mechanisms of aggregation are being affected exactly. Following suit with previous experiments performed in this study, a T119W mutation was introduced into m-TTR and samples were incubated at a pH of 4.4 and a temperature of 4 °C. Interestingly, a nearly homogenous solution of tetrameric protein was observed upon initial injections with very minute amounts of monomer already becoming present. This observation is most likely attributed to the tryptophan mutation being introduced in such close proximity to the L110M mutation of the m-TTR, allowing the m-T119W-TTR to form into its tetrameric native state. After the initial 24 hours of incubation more than 90% of the protein had dissociated into its monomeric constituents with minute amounts of dimer being formed (Figure 3.8, Day 1). Day 2 injections revealed that the remaining tetramers continued to dissociate into monomers, as the monomeric concentrations increase slightly, while the dimer concentrations remain relatively small and are consistent with the previous day's injection (Figure 3.8). By this point in the aggregation of the unmutated m-TTR from Figure 3.6, it can be expected that a period of accelerated dimer formation has occurred. The absence of any meaningful concentrations of dimer indicates that the T119W mutation introduced into the m-TTR has effectively blocked dimer formation. This pattern continues throughout Day 3 as the tetramers were shown to be nearly depleted, giving rise to the highest concentration of monomer and still only a slight increase in dimeric species over the course of the study (Figure 3.8). Interestingly, comparisons may now be drawn between the aggregation kinetics of Figure 3.7, in which the aggregation process was all but halted, and the structural characterizations of Figure 3.8, where a complete

absence of oligomers was observed. This lack of oligomerization may be attributed to the noticeable lack of dimers observed in Figure 3.8.

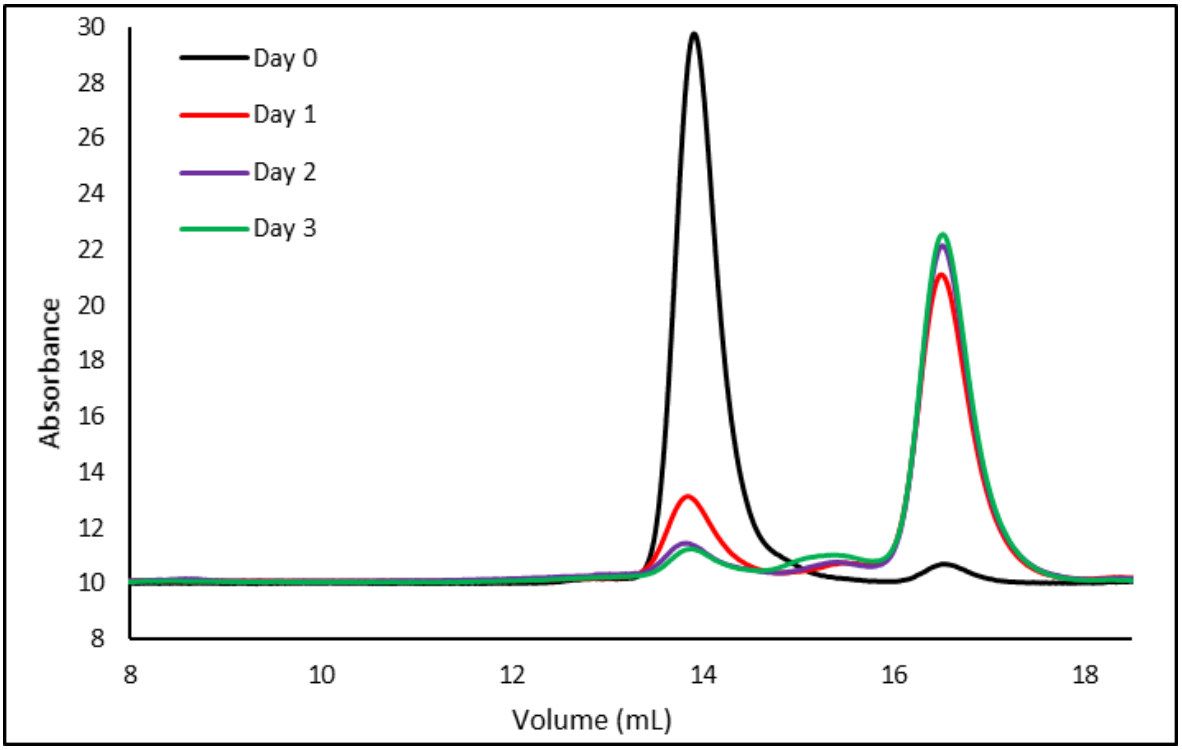

Figure 3.8 SEC profile of m-T119W-TTR incubated at 0.2 mg/mL, a pH of 4.4, and at 4 °C for three days. Similarly to the WT, V30M, and L55P-TTR studies, tetrameric conformations were observed in the 13.5 mL – 15.0 mL elution volume range, dimeric conformations in the 15.0 mL – 16.0 mL range, and monomeric conformations in the 16.0 mL – 17.5 mL range. A noticeable lack of high molecular weight species (<13.5 mL) can be observed.

3.6 Proline substitution of the E92 peptide in the F-strand of m-TTR blocks oligomer formation during the aggregation process

For comparative analysis of how the E92P point mutation affects the aggregation of non-native amyloidogenic species within m-TTR as to that of WT-TTR, studies were performed on m-TTR under acidic conditions and while proteolytically cleaved at a neutral pH, similar to those of Figure 3.5. Samples incubated under perturbation in highly acidic conditions resulted in familiar trends to those of Figure 3.5 and 3.6, with the E92P samples exhibiting greatly reduced oligomerization, nearly halting the process altogether (Figure 3.9, top). Interestingly, the observed kinetics of the proteolytically cleaved samples incubated under neutral pH deviated from those of the WT study. All though the cleaved samples still aggregated, they plateaued after 24 hours whereas their WT counterparts continued aggregation, indicating that an equilibrium had been reached within the E92P kinetic pathway (Figure 3.9, bottom). To gain insight into how the natural aggregation process of m-TTR is being altered by the E92P mutation structurally, samples of m-TTR-E92P were incubated under similar conditions as to those in Figure 3.9 and subjected to analysis via SEC. Initial injections performed immediately upon denaturation of the protein samples produced an SEC profile consisting mainly of monomeric species with small amounts of dimers already in the early stages of development (Figure 3.10, Day 0). Comparing this Day 0 profile with what was expected from the reference m-TTR set in Figure 3.7, it can be seen that there are already small differences in the amounts of dimeric and oligomeric species. Whereas the m-TTR has a miniscule amount of dimers present with even less oligomers, the E92P sample has a higher initial dimer concentration with a noticeable lack of oligomeric presence. This absence of oligomers continues over the course of the study as subsequent day's injections reveal a decreasing monomeric concentration coinciding with slow increases to the dimeric species, eventually reaching each of the previously

described equilibrium stages between the two species while never entering into the oligomeric production stage of the aggregation process.

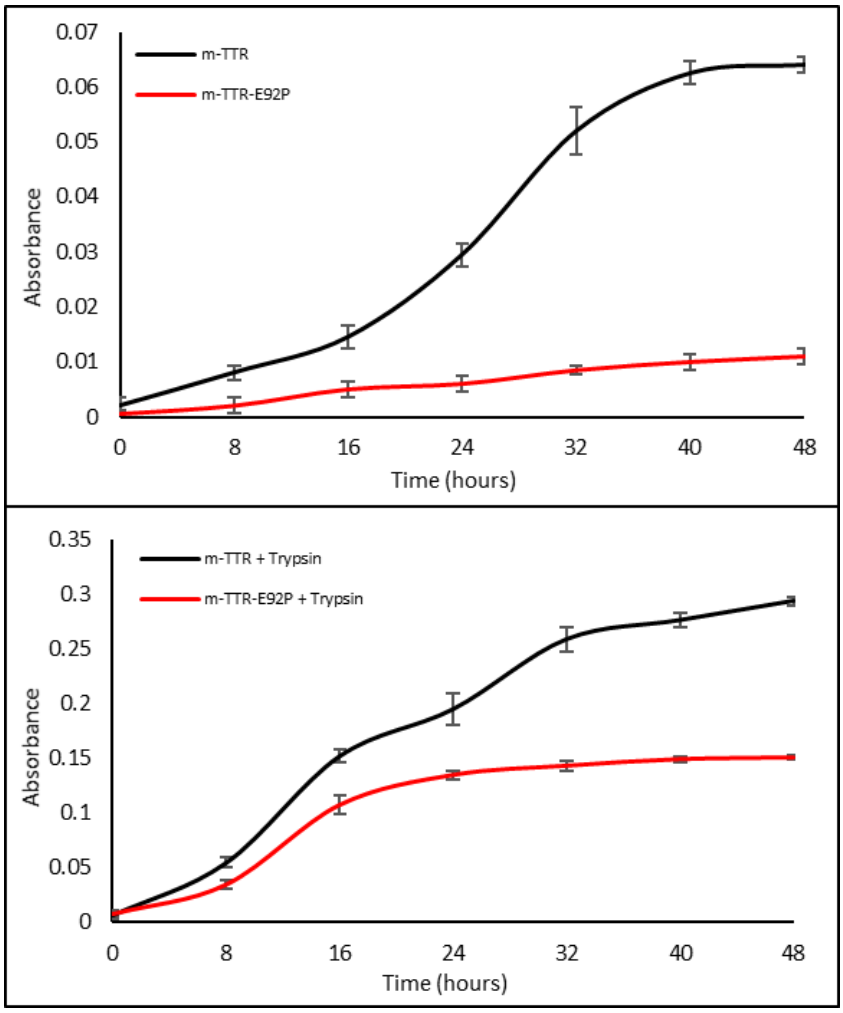

Figure 3.9 Aggregation kinetics observed at an OD_{400} of m-TTR with the E92P mutation at 37 °C. Samples incubated at a pH of 4.4 with shaking (top). Samples incubated at a pH of 7.4 with trypsin while shaking (bottom).

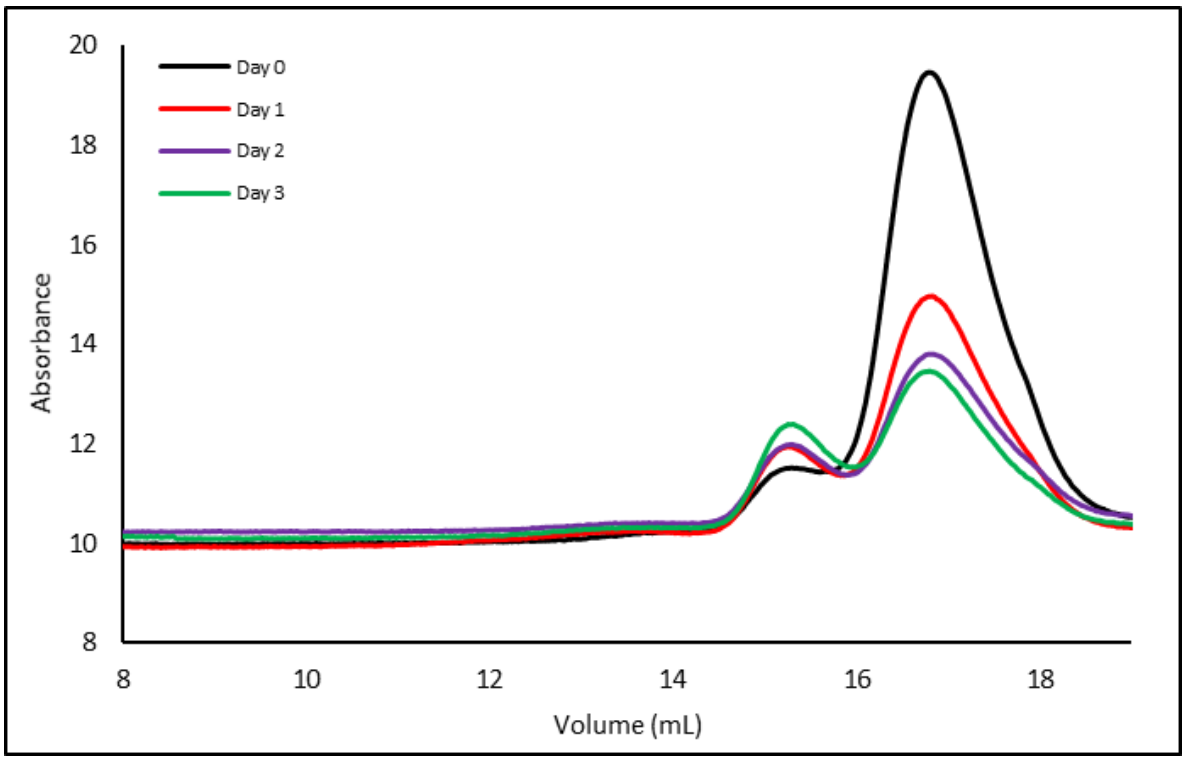

Figure 3.10 SEC profile of m-E92P-TTR incubated at 0.2 mg/mL, a pH of 4.4, and at 4 °C for three days. Monomeric conformations were observed in the 16.0 mL – 18.0 mL elution volume range and dimeric conformations in the 15.0 mL – 16.0 mL range. A noticeable lack of high molecular weight oligomeric conformations may be observed in the 11.0 mL – 14.0 mL elution volume range.

3.7 Mutations T119W and E92P are capable of inhibiting oligomerization in the highly amyloidogenic L55P-TTR variant commonly associated with FAP

As a point of interest for future studies, this study aimed to elicit whether the inhibition of oligomeric species brought upon by sterically hindering select bonding sites within the F and H β-strands affect mutated TTR species most predominantly associated with FAP, such as those of L55P-TTR.[14] Of all the proteins associated with FAP, L55P is considered to be the most aggressive when it comes to disease pathology and progression.[14,17] To build an initial correlation between the amyloidogenesis of L55P and those of the native WT and m-TTR species as conceptual proof, the aggregation kinetics of L55P and those of the native state and a monomeric variety performed previously would need to be compared. This correlation was accomplished by replicating environmental and physiological conditions under which the studies in Figure's 3.4, 3.5, and 3.6 were performed for samples of L55P-TTR with the mutations T119W and E92P introduced. Upon analysis, it was observed that the aggregation kinetics of both the L55P and L55P-T119W at a pH of 4.4 (Figure 3.11, top) and those of the cleaved samples incubated at neutral pH (Figure 3.11, bottom) followed nearly identical aggregation patterns as those in the WT-TTR studies (Figure 3.4). These similarities indicate that the T119W mutation is capable of preventing even one of the most highly amyloidogenic species from aggregating into oligomeric species, pointing towards a key mechanism of the amyloidosis process being blocked through perturbation of the H-strand. Complimenting this data, studies were also performed upon the aggregation kinetics of L55P-TTR affected by the E92P mutation of the F-strand (Figure 3.12). Much like the T119W results, the E92P mutations also showed similar aggregation kinetics to those of its WT and m-TTR counterparts, with the main difference once again being that the E92P samples are still capable of, all though at a greatly reduced rate, oligomerizing. Taken together, the results from Figures 3.11 and 3.12, compared to those

performed on WT and m-TTR, allude to a mutation independent mechanism being affected which either greatly reduces or completely eliminates oligomer aggregation.

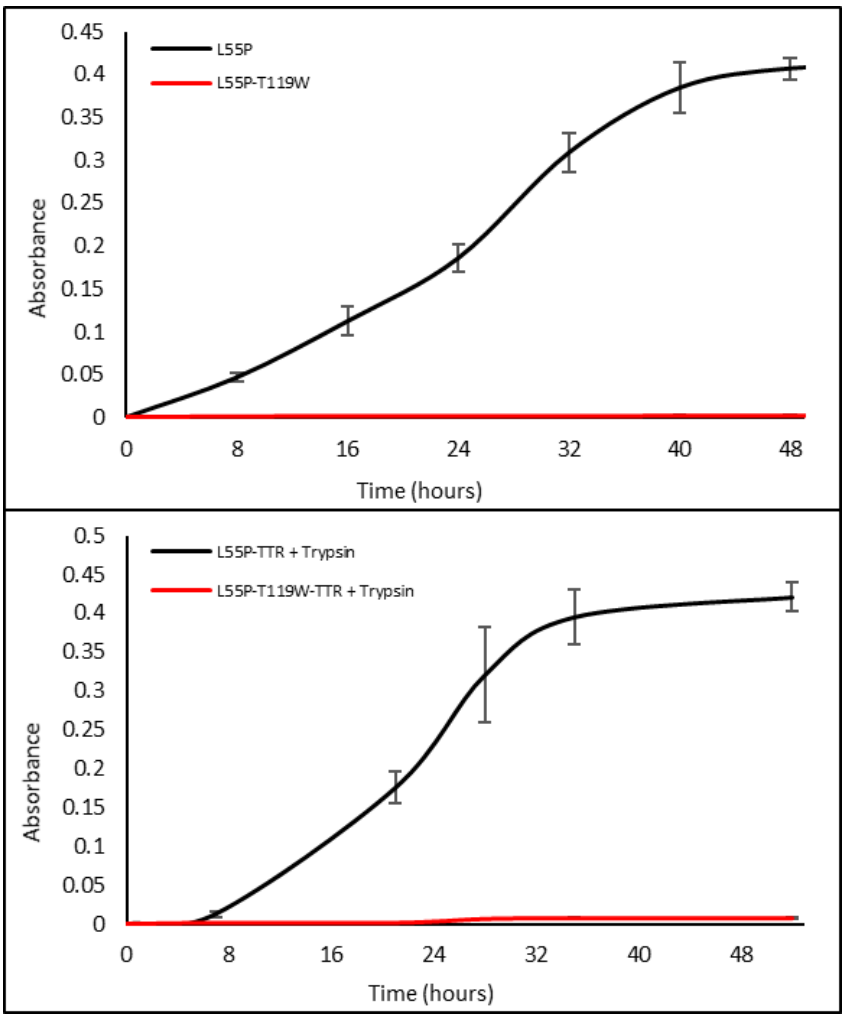

Figure 3.11 Aggregation kinetics observed at an OD_{400} of L55P-TTR with the T119W mutation at 37 °C. Samples incubated at a pH of 4.4 with shaking (top). Samples incubated at a pH of 7.4 with trypsin (bottom).

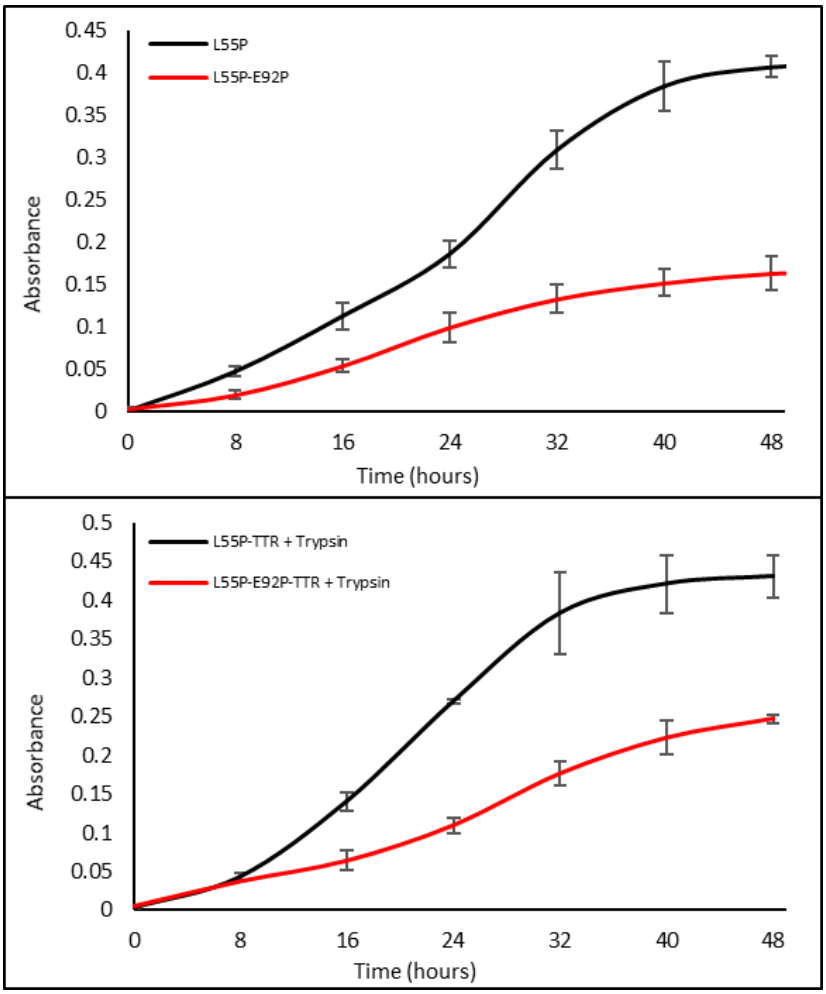

Figure 3.12 Aggregation kinetics observed at an OD_{400} of L55P-TTR with the E92P mutation at 37 °C. Samples incubated at a pH of 4.4 with shaking (top). Samples incubated at a pH of 7.4 with trypsin (bottom).

Chapter 4: Discussion and Conclusion

The underlying mechanisms associated with protein dissociation, misfolding, and subsequent aggregation within ATTR are intricately complex with little actually known about the specific pathways enveloped within the process of amyloidogenesis. Many studies have been performed with the goal of finding prospective aggregation pathways in an aim towards developing a more strictly defined structural evolution of amyloidogenic species. Of such studies, there exists strong data which suggests that the dimeric intermediaries formed upon the aggregation of misfolded monomers play essential roles in the process of amyloidosis.[3,6,7] To further clarify the involvement of these dimeric states within ATTR, these set of studies sought to introduce mutations which inhibited the formation of monomeric TTR's most accessible bond interface located at the H to H' and F to F' β-strand bonds. Tryptophan and proline mutations, which are inherently bulky in nature, were introduced into wild type, monomeric, and L55P-TTR through site directed mutagenesis in order to introduce unfavorable steric hinderances within the tightly interdigitated hydrogen bonds of the monomer-to-monomer interface region.

Upon initial examination of the intermediate species which form in the early stages of amyloidogenesis, it was observed that as the native tetramer of WT-TTR dissociated into its constituent monomers, dimeric species began to arise in subsequent days, eventually leading to large concentrations of high molecular weight oligomers after 1 week (Figure 3.1). As WT-TTR is only associated with one of the three common forms of ATTR, SSA, the most prevalently found mutations of FAP/FAC, V30M and L55P, were also studied in hopes of revealing commonalities in the oligomerization process involving dimerization. Observations of the oligomerization behavior of these two mutants yielded similar patterns to those of WT-TTR, albeit with an expected increase in the rate of the aggregation kinetics of the V30M samples (Figure 3.2) and a much larger increase in the rate of oligomerization within the L55P samples (Figure 3.3). These two naturally occurring mutations have been previously shown to undergo a

uniquely aggressive amyloidogenesis which is supported by these results.[14,25] To assess if the introduction of the T119W and E92P mutations had any impact on the aggregation processes of WT-TTR, a pair of studies were performed for each species under different physiological conditions favorable for amyloidogenesis. The WT-T119W species achieved near complete inhibition of oligomeric species when incubated at a pH of 4.4 and interestingly as well in the proteolytically cleaved samples incubated at a neutral pH, which exhibit increased aggregation kinetics (Figure 3.4).[5] Comparatively, the WT-E92P samples were also able to achieve inhibition of oligomerization to near completion in the pH 4.4 samples, however, a difference between the two arose as the E92P samples incubated with trypsin at a neutral pH were still able to aggregate, though at a slower rate (Figure 3.5). These sets of observations appear to place an emphasis on the relevance of the H β-strand in forming dimeric species compared to that of the F β-strand, perhaps arising from the close proximity of the more thoroughly interdigitated hydrogen bonds within the H β-strand compared to those of the F β-strand (Figure 1.6). Overall, the T119W mutation appears to be the more effective inhibitor, however, both mutations show great potential towards being further developed into possible therapeutical remedies.

In order to further narrow down the possible aggregation pathways occurring during incubation, m-TTR was implemented as a means of bypassing the rate-limiting step of tetrameric dissociation in the native state of TTR. By doing so, one of the two possible dimeric generation phases is eliminated, allowing for scrutiny of only species which arise during the aggregation process, rather than those that could also be forming during the tetrameric dissociation stage. It was found that the highly destabilized tetramer of the m-TTR mutant immediately dissociated into its monomeric constituents upon denaturation with minute amounts of dimer already being recognizable (Figure 3.7). Over the course of the next three days, the concentrations of monomers continued to decrease as, initially, the dimeric concentrations increase with subsequent increases in high molecular weight oligomer concentrations. This

pattern shares expected similarities to those of misfolded monomers of native WT-TTR post dissociation, as they first form dimers which are then followed by oligomers. Replicating the discovery process of the WT studies, a T119W mutation was then introduced into m-TTR and pairs of samples were incubated under different physiological conditions for aggregation kinetics observations (Figure 3.6). Nearly identical patterns of inhibition with the T119W mutations were observed in the m-TTR sample sets compared to those of the WT-TTR in Figure 3.4. This observation may be attributed to the inability of both m-TTR's and WT-TTR's aggregate prone monomers to form dimeric species upon aggregation leading to diminished oligomer formation. For further insight into which species were developing during aggregation, size exclusion chromatography was utilized with samples incubated under similar physiological conditions as those of the WT-TTR and m-TTR (Figure 3.8). Interestingly, the m-T119W-TTR did not immediately dissociate upon denaturation as the m-TTR samples had, remaining largely in its tetrameric state upon initial injection, suggesting this secondary mutation may have a stabilizing affect upon the F87M-L110M mutations of the m-TTR variant. After 24 hours, a majority of the proteins in their native state had dissociated into monomers, with small amounts of dimers forming. Over the next two days, the remaining amounts of tetramer continue to dissociate into more monomers, while dimer concentrations remain nearly constant, and no oligomers arise. These observations allude to the dimeric intermediaries playing key roles in the formation of oligomers, as their formation has been verified to be hindered and this coincides with a noticeable absence of oligomers. Continuing the discovery process for the WT studies, E92P was also introduced individually into m-TTR to observe any effects this may have on oligomerization. Much like the T119W studies, the E92P mutation appeared to completely block the oligomerization process, however, it was capable of forming higher concentration of dimeric species compared to its T119W counterpart. To further justify the dimeric inhibition theory as well as provide a point of interest for future research related to ATTR and the oligomerization process as a whole, kinetics studies were also performed on the highly amyloidogenic L55P-

TTR species with the introduction of the T119W and E92P mutations. The correlation established between the kinetics of the L55P samples in Figure 3.11, Figure 3.12, and those of the WT-TTR and m-TTR samples previously examined within this study suggests strongly that the T119W and E92P inhibition mechanisms are species independent, blocking a common path through which all oligomers are formed during amyloidogenesis, that of which being their ability to form dimeric intermediaries.

It has been demonstrated by this study that the oligomerization pathway within ATTR is reliant upon the capability of its constituent misfolded monomers to evolve into dimeric states which are then capable of driving further aggregation into high molecular weight oligomers. This has led to the conclusion that the mechanism through which oligomeric species first arise in the aggregation process involves a clear dependence upon the concentration of dimeric species in solution. Inhibition of TTR's ability to form stable dimeric species was accomplished through introducing tryptophan and proline point mutations into the H and F β-strands. These mutations achieved an inhibitory affect due to their bulky nature, sterically hindering the tightly interdigitated hydrogen bonds located within the H to H' and F to F' dimeric interface. The overall inhibitory mechanism was found to be successful within even one of the most highly amyloidogenic species of TTR, L55P, suggesting that mutated species of TTR undergo the same process of amyloidosis as their WT counterparts.

References

1. Benson, M. et al. (2020). Amyloid nomenclature 2020: update and recommendations by the International Society of Amyloidosis (ISA) nomenclature committee. Amyloid, 27(4), 217-222.
2. Benson, M. & Uemichi, T. (1996). Transthyretin Amyloidosis. Amyloid, 3(1), 44-56.
3. Blake, C. et al. (1978) Structure of Prealbumin Secondary, Tertiary and Quaternary Interactions Determined by Fourier Refinement at 1.8 Å. Journal of Molecular Biology, 121, 339-356.
4. Connolly, M. et al. (2019). Estimating the fiscal impact of rare diseases using a public economic framework: a case study applied to hereditary transthyretin mediated (hATTR) amyloidosis. Orphanet Journal of Rare Diseases, 14(220).
5. Dasari, A. et al. (2020). Disruption of the CD Loop by Enzymatic Cleavage Promotes the Formation of Toxic Transthyretin Oligomers through a Common Transthyretin Misfolding Pathway. Biochemistry, 59, 2319-2327.
6. Dasari, A. et al. (2019). Transthyretin Aggregation Pathway toward the Formation of Distinct Cytotoxic Oligomers. Scientific Reports, 9(33).
7. Dasari, A. et al. (2019) Two Distinct Aggregation Pathways in TTR Misfolding and Amyloid Formation. Biochimica et Biophysica Acta (BBA) - Proteins and Proteomics. 1867(3), 344-349.
8. Dharmarajen, K. et al. Transthyretin Cardiac Amyloidoses in Older North Americans. Journal of the American Geriatrics Society, 60(4), 765-774.
9. Foss, T. et al. (2005). The Pathway by Which the Tetrameric Protein Transthyretin Dissociates. Biochemistry, 44, 15525-15533.

10. Gonzalez-Duarte, A., & Ulloa-Aguirre, A. (2021). A Brief Journey through Protein Misfolding in Transthyretin Amyloidosis (ATTR Amyloidosis). International Journal of Molecular Science, 22, 13158.
11. Hurshman, A. et al. (2004) Transthyretin Aggregation under Partially Denaturing Conditions is a Downhill Polymerization. Biochemistry, 43, 7365-7381.
12. Ivanova, M. et al. (2013) Aggregation-triggering segments of SOD1 fibril formation support a common pathway for familial and sporadic ALS. PNAS, 111(1), 197-201.
13. Ke, P. et al. (2020) Half a century of amyloids: past, present and future. Chemical Society Revenue, 49, 5473-5509.
14. Keech, C. et al. (2005). L55P Transthyretin Accelerates Subunit Exchange and Leads to Rapid Formation of Hybrid Tetramers. The Journal of Biological Chemistry, 280(50), 41667-41674.
15. Lashuel, H. et al. (1998) Characterization of the Transthyretin Acid Denaturation Pathways by Analytical Ultracentrifugation: Implications for Wild-Type, V30M, and L55P Amyloid Fibril Formation. Biochemistry, 37, 17851-17864.
16. Lashuel, H. et al. (1999) The Most Pathogenic Transthyretin Variant, L55P, Forms Amyloid Fibrils under Acidic Conditions and Protofilaments under Physiological Conditions. Biochemistry, 38, 13560-13573.
17. Lim, K. et al. (2017) Pathogenic Mutations Induce Partial Structural Changes in Native β-Sheet Structure of Transthyretin and Accelerate Aggregation. Biochemistry, 56(36), 4808-4818.
18. Mangione, P. et al. (2014) Proteolytic cleavage of Ser52Pro variant transthyretin triggers its amyloid fibrillogenesis. Proceedings of the National Academy of Sciences of the United States of America, 111(4), 1539-1544.

19. Muntau, A. et al. (2014) Innovative strategies to treat protein misfolding in inborn errors of metabolism: pharmacological chaperones and proteostasis regulators. Journal of Inherited Metabolic Diseases, 37(4), 505-523.
20. Pacini, L. et al. (2020) Induced Perturbation Network and tiling for modeling the L55P Transthyretin amyloid fiber. Procedia Computer Science, 178, 8-17.
21. Saelices, L. et al. (2017). Amyloid seeding of transthyretin by ex vivo cardiac fibrils and its inhibition. PNAS, 115(29), 6741-6750.
22. Saelices, L. et al. (2018) Crystal structures of amyloidogenic segments of human transthyretin. Protein Science, 27, 1295-1303.
23. Saelices, L. et al. (2015) Uncovering the Mechanism of Aggregation of Human Transthyretin. The Journal of Biological Chemistry, 290(48), 28932-28943.
24. Sawaya, M. et al. (2007) Atomic structures of amyloid cross-b spines reveal varied steric zippers. Nature, 447, 453-457.
25. Schmidt, M. et al. (2019) Cryo-EM structure of a transthyretin-derived amyloid fibril from a patient with hereditary ATTR amyloidosis. Nature Communications, 10(1), 1-9.
26. Sun, X. et al. (2018) Kinetic analysis of the multistep aggregation pathway of human transthyretin. PNAS, 115(27), 6201-6208.